THE EFFECTS OF NON-THERMAL VELOCITY FIELDS ON SOLAR LINE PROFILES

by

LAWRENCE WILLIAM RAMSEY

B.A., University of Missouri, St. Louis, 1968

9984

A MASTER'S THESIS

submitted in partial fulfillment of the

requirements for the degree

MASTER OF SCIENCE

Department of Physics

KANSAS STATE UNIVERSITY

Manhattan, Kansas

1972

Approved by:

J. C. Evans

Major Professor

THIS BOOK CONTAINS NUMEROUS PAGES WITH THE ORIGINAL PRINTING BEING SKEWED DIFFERENTLY FROM THE TOP OF THE PAGE TO THE BOTTOM.

THIS IS AS RECEIVED FROM THE CUSTOMER.

TABLE OF CONTENTS

Page

I. INTRODUCTION 1

II. LINE FORMATION IN NON-THERMAL VELOCITY FIELDS 4

a) Classical Line Formation 4
b) Optically Thin Scale of Non-thermal Velocity Fields--Microturbulence 6
c) Optically Thick Scale of Velocity Fields--Macroturbulence 9

III. NON-THERMAL VELOCITY FIELD MODELS 19

a) Observed Solar Velocity Fields 19
b) Optically Thin Velocity Field Models 21
c) Optically Thick Velocity Field Models 24

IV. NUMERICAL RESULTS FOR THE VARIOUS MODELS ON SOLAR INTENSITY LINE SHAPES 29

a) Curve of Line Shape Diagram 29
b) Optically Thin Velocity Fields 33
c) Optically Thick Velocity Fields 43

V. RESULTS FOR FLUX LINE SHAPES 51

VI. CONCLUSIONS 55

REFERENCES 58

APPENDICES

A. STELLAR LINE FORMATION THEORY 60

a) Line Depth Calculation 60
b) Curve of Growth Theory 66

B. NUMERICAL INTEGRATION OF INTENSITY PROFILES 69

LIST OF TABLES

Table		Page
1	Atmospheric Abundances* for Solar Model	5
2	Atomic Parameters	7
3	Solar Microturbulence Determinations	19

LIST OF FIGURES

Figure		Page
1	Cell Structure of Velocity Field Element	10
2	Optically Thin Velocity Field Models	23
3	Area-Velocity Spectrums	23
4	Semi-Empirical Optically Thick Velocity Field Model	27
5	Curve of Growth--Curve of Line Shape Correlation	32
6	Theoretical Curve of Line Width for FeI (1) λ5250	35
7	Theoretical Curve of Growth for FeI (1) λ5250	35
8	Classical Microturbulence Curves of Line Shape FeI (1) λ5250	38
9	Classical Microturbulence Curve of Line Shape FeI (687) λ4863	38
10	Microturbulence Line Profiles	40
11	Curve of Line Shape for Utrecht Model	42
12	Curve of Line Shape for Schmalberger Model	42
13	Curve of Line Shape for 1HG Model with $\mu = 1.00$	45
14	Curve of Line Shape for 1HD Model with $\mu = 1.00$	45
15	Curve of Line Shape for Isotropic Model with $\mu = 0.40$	48
16	Curve of Line Shape for Anisotropic Model with $\mu = 0.40$	48

Figure | Page

Figure		Page
17	Optically Thick Velocity Field Line Profiles	50
18	Curve of Line Shape for Schmalberger Model in Flux	53
19	Curve of Line Shape for Anisotropic Model in Flux	53
20	Empirical Curve of Line Shape for τ Scorpii	57
B1	Integrand Curves	72
B2	Error Data For 5 and 10 Point Integration	72
B3	Error Data For 3 Point Integrations....................	78
B4	Error Data For 4 Point Integrations....................	78

ACKNOWLEDGMENT

The author would like to thank Dr. J. C. Evans of the Physics Department for suggesting the problem and his guidance throughout this study. I would also like to express my appreciation to the University Computing Center for their cooperation. Not least, I would like to thank my wife who did much of the data tabulation used in this paper.

I. INTRODUCTION

Traditionally, stellar spectroscopists have considered two distinct scale sizes for non-thermal velocity fields in explaining the observed shifts and shapes of stellar spectral lines. The distinction between these fields has been made according to the geometrical scale of the mass motion relative to a photon mean free path in the medium. The non-thermal velocity fields for which characteristic sizes are smaller than a photon mean free path are commonly called microturbulence and those for which the characteristic sizes are larger are known as macroturbulence.

The concept of the small scale velocity fields was first introduced by Struve and Morgan (1932) and Elvey (1934) and was first applied in the analysis of a stellar spectrum by Struve and Elvey (1934). The large scale velocity fields were first considered observationally by Struve (1946) and the theoretical implications were detailed by Unsold and Struve (1949). Struve called these motions "turbulence"; however, pointing out that the motions may be of a streaming nature and thus caution should be used in the physical interpretation of the word turbulence. The effects of large scale and small scale velocity fields on stellar spectra have been studied in some detail by Huang and Struve (1952, 1955) using the curve of line width method. A summary of their ideas and more extensive references are given in the review given by Huang and Struve (1960). A review of the observational evidence for velocity fields in stellar atmospheres, which unfortunately is confined giant and supergiant stars, is given by Underhill (1961). The actual investigation of the shapes of stellar line profiles has been done by several researchers.

Huang and Struve (1953) used several models of large scale velocity fields in an attempt to fit the profiles of ρ Leonis. Slettebak (1956) used a similar approach in an unsuccessful attempt to distinguish the effects of rotation and large scale motions. Abt (1958) considered macroturbulence in a study of line broadening in supergiants and more recently Scholz (1972) considers macroturbulence as a major line broadening mechanism in the atmospheres of O stars. In the case of the sun, high quality spectrophotometric data allows detailed study of line profile shapes. Elste (1967) and Gurovenko and Ratnikova (1971) have shown the importance of allowing for large scale velocity fields in solar line profile analysis. deJager and Neven (1967) have shown how much data can be used to deduce the small and large scale velocity fields and Gonczi and Roddier (1971) have proposed a model for the solar velocity fields using the 4607A line of SrI. This list is certainly not exhaustive, especially in the solar case.

Also of significance is the recent resurrection of serious questions by Worrall and Wilson (1972a, 1972b) concerning the physical nature, and indeed the very existance, of small scale velocity fields as presently used. As none of the cited investigations have critically compared line profiles due to large scale and small scale velocity fields, it would seem useful to discuss theoretically what qualitative and quantitative differences one might expect.

In this investigation we have studied separately the effects of both small and large scale velocity fields on line profiles. We have attempted to show that lines formed in a pure small scale velocity field are qualitatively and quantitatively different than those formed in a purely large scale velocity field. Of course we do not contend that either scale of velocity field is solely active in the sun or in any other star. It is felt that the information from such a segregation will aid in choosing a direction for studying the much more complex situation which exists in the atmospheres of stars and in the solar photosphere.

It seems desirable to change the terminology so as to be unambiguous about the processes involved. There is certainly some question as to whether the phenomenon we refer to as turbulence is in reality turbulence in an aerodynamic sense (Huang and Struve, 1960; Clauser, 1961). In aerodynamics, turbulence is described as a random and fluctuating motion which occurs when the viscous forces are no longer sufficiently strong to damp out the small scale oscillations which are always present (Lin and Reid, 1963). A more precise description of the phenomenon in stellar atmosphere would be to call the small and large scale motions optically thin velocity fields and optically thick velocity fields, respectively.

II. LINE FORMATION IN NON-THERMAL VELOCITY FIELDS

a) Classical Line Formation

The classical problem of stellar line formation is one in which the lines are assumed to be formed by a mechanism of pure absorption in a homogeneous, steady-state, plane-parallel atmosphere in hydrostatic and radiative equilibrium. In this study, the model atmosphere used is a solar model based on an empirical temperature distribution due to Elste (1967) rather than enforcing radiative equilibrium. The model is characterized by an effective temperature of 5780°K, a surface gravity of 4.44 dex, and element abundance as given in Table 1. The continuous absorption coefficient includes the effects of bound-free and free-free transitions in H, H^-, H_2^+ and several neutral metals (Elste, 1968). The exact choice of model is not critical to this study since no attempt is made to fit observed line profiles. We shall assume that the gas is in a state of local thermodynamic equilibrium, LTE (see Appendix A).

The line profile is defined by the line depth as a function of the wavelength difference from the line center where the monochromatic continuum and line intensities are solutions of the transfer equation for a semi-infinite atmosphere (Cowley, 1970). The form of the line depth equation employed is the Planckian gradient.

Table 1

Atmospheric Abundances* for Solar Model

Element	log	Element	log
H	0.00	Si	-4.45
He	-1.00	S	-4.75
C	-3.40	K	-7.30
N	-4.00	Ca	-5.70
0	-3.10	Cr	-6.65
Na	-5.80	Fe	-4.50
Mg	-4.50	Ni	-6.00
Al	-5.60		

* The abundances are expressed as the logarithm of the number density of the element to that for hydrogen.

$$r(\mu) = \int_{-\infty}^{\infty} \frac{1}{I^c} \frac{dB}{dx} e^{-\tau^c/\mu} \left[1 - e^{-\tau^l/\mu} \right] dx \, , \qquad (1)$$

where x is the logrithm of the monochromatic continuum optical depth at 5000 A. The symbols all have their usual meaning (see Appendix A). The line absorption coefficient per hydrogen particle, K^l , can be calculated in terms of the voigt function, H(a,v),

$$\kappa^{l} = \left(1 - e^{-hc/\lambda kT}\right) \frac{N}{N_H} \frac{\sqrt{\pi}}{m_e c} \frac{\lambda^2}{\Delta\lambda_D} f\, H(a,v)\,, \tag{2}$$

where $\left(1 - e^{-hc/\lambda kT}\right)$ is the correction for stimulated emission, N/N_H the ratio of atoms in the lower level of the transition of interest to the number of hydrogen particles, $\Delta\lambda_D$ is the doppler width and is given by

$$\Delta\lambda_D = \frac{\lambda}{c}\sqrt{\frac{2kT}{m}}\,, \tag{3}$$

and f is the oscillator strength. The damping parameter, a, includes natural broadening due to radiation damping, quadratic Stark broadening due to electrons and ions, and a van der Waah broadening due to interactions with hydrogen and hilium. The remaining symbols have their usual meaning. Table 2 gives the atomic parameters of the lines used in this study.

b) <u>Optically Thin Scale of Non-thermal Velocity Fields--Microturbulence</u>

The optically thin scale of velocity fields will be taken to mean those non-thermal motions whose dimensions are less than or on the order of the mean free path of a photon. The mean free path is the reciprocal of the product of the mass absorption coefficient and the density,

$$l = {}^1/\kappa\rho \,. \tag{4}$$

Table 2

Atomic Parameters

Element	Mult		lower	log gf	log χ_{rad}	2/3 $\log C_4$	2/5 $\log C_6$
Fe I	(1)	5250.21	0.12	-4.46	7.90	-8.87	-12.91
Fe I	(687)	4863.65	3.42	-1.21	7.97	-8.67	-12.47

In terms of an optical depth scale, the mean free path is a change in line optical depth of order unity ($\Delta\tau = 1$). Typical path lengths in the solar photosphere (which is about 500 km thick) are on the order of 2 km in deep layers, 30 km in the weak line formation region, and several hundred kilometers in the high photosphere.

This scale of velocity fields includes the "classical microturbulence" as introduced by Struve and Elvey (1934). By classical microturbulence, we shall mean an optically thin velocity field which is isotropic and homogeneous with depth having a Gaussian velocity distribution along the line of sight. The classical microturbulence produces a Gaussian shape for the line absorption coefficient which results from the convolution of the Gaussian profiles of the thermal and turbulent broadening (Cowley, 1970). Therefore the doppler width will include a term ξ , whose value is that of the most probable velocity of the distribution. Therefore equation (3) becomes with the inclusion of classical microturbulence

$$\Delta\lambda_D = \frac{\lambda}{c}\sqrt{\frac{2kT}{m} + \xi^2} \, . \tag{5}$$

Huang (1950) has considered other distributions than Gaussian, but virtually all investigations, including those using depth dependent anisotropic models, have assumed the Maxwellian distribution function.

In addition to classical microturbulency we have considered in this study broadening due to both a depth dependent radial and tangential velocity components, ξ_r and ξ_t , respectively. The most probable velocity, ξ , is then given by

$$\xi^2 = \xi_r^2 \mu^2 + \xi_t^2 (1-\mu^2) \, , \tag{6}$$

where μ (= $\cos\Theta$) is the limb distance and Θ is the angle between the line of sight and the radial direction. Hence, an optically thin velocity field is parameterized by the depth dependence of the radial and tangential components of the most probable velocity for the assumed distribution function (a Gaussian).

c) Optically Thick Scale of Velocity Fields--Macroturbulence

We shall now obtain a general expression for line depth which includes the effects of optically thick velocity fields. These velocity fields are large scale motions whose dimensions are on the order of the size of the photosphere or, more precisely, larger than a photon mean free path. An alternate way of finding the final line profile, $r'(x)$, is by convoluting a zero velocity line profile, $r(x)$, with a broadening function, $B(x)$, which is derived from the velocity distribution of the large scale field (Huang and Struve, 1953, 1960; Slettebak, 1956; Abt, 1958). If $B(x)$ is normalized, we have

$$r'(x) = \int_{-\infty}^{\infty} B(x-y)\, r(y)\, dy. \tag{7}$$

This technique was not used as it requires a derivation of a new broadening function, $B(x)$, from the geometry of each attempted model.

We shall assume that the mass motions, or optically thick velocity fields, are cellular in nature and do not destroy the general overall hydrostatic equilibrium of the atmosphere. Consider a unit area A positioned at some limb distance as shown in Figure 1. This area is composed of n smaller elements, each of area a_i, where a_i is defined as the fraction of A occupied by elements with velocity S_i. Thus the sum of all fractional areas is

THIS BOOK CONTAINS NUMEROUS PAGES WITH DIAGRAMS THAT ARE CROOKED COMPARED TO THE REST OF THE INFORMATION ON THE PAGE.

THIS IS AS RECEIVED FROM CUSTOMER.

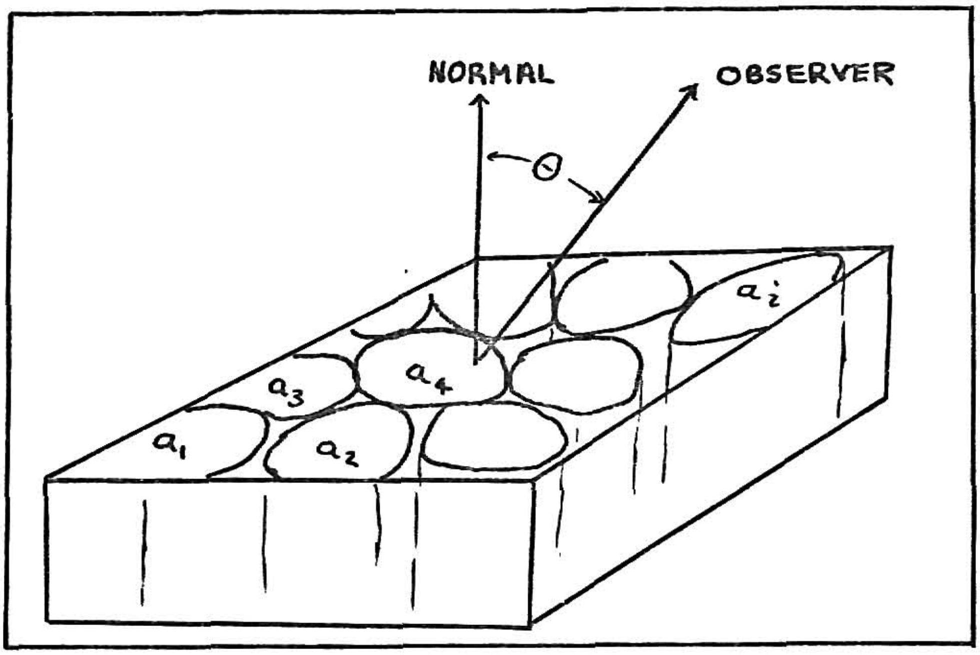

Fig. 1 - A typical area A showing the cellular pattern of an optically thick velocity field.

$$A = \sum_{i=1}^{n} a_i \equiv 1 . \tag{8}$$

We may divide the velocity along the line-of-sight into tangential components, S_t^i , and components normal to the surface, S_r^i , thus

$$S_i = S_r^i \mu + S_t^i (1-\mu^2)^{1/2} , \tag{9}$$

or in wavelength units

$$\Delta\lambda_i = \frac{\lambda}{c}\left[S_r^i \mu + S_t^i (1-\mu^2)^{1/2} \right] . \tag{10}$$

We have assumed that when intensity is measured, the slit of the spectrograph encompasses some area A containing n elements; thus individual cellular elements are not resolved. Also each element need not have the same thermal structure. This allows us to treat with this formalism the problem of an inhomogeneous atmosphere. The individual area a_i should not be thought of as representing single solar granuales but rather as the fractional area in A occupied by a particular velocity (or thermal structure).

If the continuum intensity of the i th element in I_i^c and the line intensity of that element is I_i^l , then, for A, the total monochromatic continuum intensity is the sum of the individual intensities weighted by their fractional area, or

$$I^c = \sum_{i=1}^{n} a_i I_i^c \,, \tag{11}$$

and similarily for the monochromatic line intensity

$$I^l = \sum_{i=1}^{n} a_i I_i^l \,. \tag{12}$$

If equations (11) and (12) are substituted into the line depth equation (see Appendix A) the line depth for A can be written as

$$r(\mu) = \sum_{i=1}^{n} a_i \left(I_i^c - I_i^l \right) / I^c \,, \tag{13}$$

which is equivalent to the expression

$$r(\mu) = \frac{1}{I^c} \sum_{i=1}^{n} a_i I_i^c r_i(\mu) \,, \tag{14}$$

where $r(\mu)$ is the line depth for the i th cell. It is important to note that we have combined the emitted intensities from each cell and have not considered the problem of the transfer of radiation through adjacent cells as would be the actual case as one approaches the limb. Writing the continuum intensity as the solution of the transfer equation for the area a_i we have

$$I_i^c = \int_{-\infty}^{\infty} S_i^c \, e^{-\tau_i^c/\mu} \left(\frac{K_i^c}{K_o}\right)\left(\frac{10^x}{Mod}\right) \frac{dx}{\mu} , \tag{15}$$

where S_i^c in the continuum source function in area a_i, K_i^c is the continuous absorption coefficient in a_i, K_o is the continuous absorption coefficient in an ambient reference photospheric cell, Mod is $\log_{10}e$, τ_i^c is the continuum optical depth in area a_i which is given by

$$\tau_i^c = \int_{-\infty}^{x} \frac{K_i^c}{K_o} \left(\frac{10^x}{Mod}\right) dx , \tag{16}$$

and x is as before. Similarly for the solution to the line transfer equation for area a_i we have

$$I_i^l = \int_{-\infty}^{\infty} S_i \, e^{-\tau_i/\mu} (1+\eta_i) \left(\frac{K_i^c}{K_0}\right)\left(\frac{10^x}{Mod}\right) \frac{dx}{\mu} \,, \tag{17}$$

where

$$S_i = (S_i^c + \eta_i S_i^l)/(1+\eta_i) \,, \tag{18}$$

and
$$\tau_i = \tau_i^c + \tau_i^l . \tag{19}$$

In equation (18) S_i^l is the line source function for area a_i and η_i is the ratio of the line absorption coefficient to the continuous absorption coefficient in area a_i and τ_i^l in equation (19) is the line optical depth. By substituting equations (15) and (17) into the line depth equation we can obtain the expression

$$r_i(\mu) = \frac{1}{I_i^c} \int_{-\infty}^{\infty} S_i^c \, e^{-\tau_i^c/\mu} \left[1 - (1+\eta_i)\beta_i \, e^{-\tau_i^l/\mu}\right] \tag{20}$$

$$\times \left(\frac{K_i^c}{K_0}\right)\left(\frac{10^x}{Mod}\right) \frac{dx}{\mu} \,,$$

where

$$\beta = S_i^l / S_i^c \ . \tag{21}$$

The line depth in the Planckian gradient form, is

$$r(\mu) = S_i(0)\left[1 - \beta_i(0)\right] + \frac{1}{I_i^c}\int_{-\infty}^{\infty} \frac{dS_i^c}{dx}\, e^{-\tau_i^c/\mu}\left[1 - \phi\, e^{-\tau_i^l/\mu}\right] dx \,, \tag{22}$$

where

$$\phi_i = \frac{dS_i^l/dx}{dS_i^c/dx} \ . \tag{23}$$

Now, by substituting equation (20) into equation (14), we obtain the line depth for the total area A,

$$r(\mu) = \frac{1}{I^c}\sum_{i=1}^{n} \alpha_i \left\{ \int_{-\infty}^{\infty} S_i^c\, e^{-\tau_i^c/\mu}\left[1-(1+\eta)\,\beta_i\, e^{-\tau_i^l/\mu}\right] \right. \times \left(\frac{\kappa_i^c}{\kappa_0}\right)\left(\frac{10^x}{Mod}\right)\frac{dx}{\mu} \,, \tag{24}$$

and in the Planckian gradient form,

$$r(\mu) = \frac{1}{I^c} \sum_{i=1}^{n} a_i \left\{ \int_{-\infty}^{\infty} S_i^c \, e^{-\tau_i^c/\mu} \left[1-(1+\eta_i)\beta_i \, e^{-\tau_i^l/\mu}\right] \right.$$

$$\times \left(\frac{K_i^c}{K_o}\right)\left(\frac{10^x}{Mod}\right) \frac{dx}{\mu} \; , \qquad (25)$$

Equations (24) and (25) are quite general and involve no assumptions regarding the form of the source function.

It has been necessary to make the assumption of LTE in order to perform calculations which are rather lengthy. By assuming LTE, the source functions for both the line and continuum are equal to the Planck function B_i and both β_i and ϕ_i are unity. The line depth equations for the direct integration is of the form

$$r(\mu) = \frac{1}{I^c} \sum_{i=1}^{n} a_i \left\{ \int_{-\infty}^{\infty} B_i \, e^{-\tau_i^c/\mu} \left[1-(1+\eta_i) \, e^{-\tau_i^l/\mu}\right] \right.$$

$$\times \left(\frac{K_i^c}{K_o}\right)\left(\frac{10^x}{Mod}\right) \frac{dx}{\mu} \; , \qquad (26)$$

or the Planckian gradient form,

$$r(\mu) = \frac{1}{I^c} \sum_{i=1}^{n} a_i \left\{ \int_{-\infty}^{\infty} \frac{dB}{dx} e^{-\tau_i^c/\mu} \left[1 - e^{-\tau_i^l/\mu} \right] dx \right\}. \tag{27}$$

Although LTE is a highly questionable assumption for line formation, it is not crucial for this study. In the first approximation non-LTE theory modifies the atomic level populations such that they can no longer be described by a Boltzman population. In this study, theoretical curves are generated by artificially varying the elemental abundances. Therefore, the qualitative results should not be sensitive to using either a LTE or a non-LTE theory.

The second assumption which has been made to simplify the calculations was to let all the cellular areas a_i be thermally homogeneous. In this case all the I_i^c's become equal and equation (11) can be written

$$I_c = I_i^c \sum_{i=1}^{n} a_i = I_i^c . \tag{28}$$

This simplification is partially justified by the fact that the difference in continuum radiation between the bright granules and the dark inter-granular regions in the solar photosphere is small. Also, velocity differences used in this study are much too small to produce any sizeable changes in the continuum, especially in the visible, where the continuum is not strongly wavelength dependent. With this assumption the order of summation and integration may be interchanged and the line depth expressions become

$$r(\mu) = \frac{1}{I^c} \int_{-\infty}^{\infty} B \, e^{-\tau^c/\mu} \left[1 - \sum_{i=1}^{n} a_i (1+\eta_i) \, e^{-\tau_i^l/\mu} \right]$$

$$\times \left(\frac{K^c}{K_o} \right) \left(\frac{10^x}{Mod} \right) , \qquad (29)$$

or in the Planckian gradient form,

$$r(\mu) = \frac{1}{I^c} \int_{-\infty}^{\infty} \frac{dB}{dx} \, e^{-\tau^c/\mu} \left[1 - \sum_{i=1}^{n} a_i \, e^{-\tau_i^l/\mu} \right] dx . \qquad (30)$$

Equation (30) is the form utilized in this study.

III. NON-THERMAL VELOCITY FIELD MODELS

a) Observed Solar Velocity Fields

The only evidence for optically thin velocity fields in the sun is still the fact that the half-widths and equivalent widths of lines are greater than can be explained by thermal and pressure broadening alone in the context of LTE and thermal homogeneity. Even the non-LTE investigations, however, have found it necessary to incorporate an optically thin non-thermal velocity field in order to fit the high photosphereic and low chromospheric line profiles (Canfield, 1971).

Microturbulence velocity determinations from empirical solar curves of growth for FeI and FeII by Garz, et al., (1969), Yamashita (1972) and Foy (1972) yield the values displayed in Table 3.

Table 3

Solar Microturbulence Determinations

Investigator	Element	Microturbulence($^{km}/sec$)
Garz, et al.	FeI	1.00
Yamashita	FeI	1.00
	FeII	1.00
Foy	FeI	0.50
	FeII	0.65

At this point it should be pointed out that other mechanism mimic the effect of microturbulence on the curve of growth. A few of these would be Non-LTE effects (Athay & Skumanich, 1968), temperature gradients and absolute values (Pecker and Thomas, 1961), and magnetic intensification (Nichols and Evans, 1969).

Evidence for the existence of optically thick velocity fields is much more substantial. Although they are optically thin to most Fraunhofer lines, prominences are the most readily visualized phenomenon involving motion on a large geometric scale. Because of their transparency to photospheric radiation prominences are not important in this study. The solar granulation which owes its origin to the hydrogen convection zone in the envelope of the sun is perhaps the best evidence for the existence of optically thick velocity fields. Typical granual sizes range from about 700 km to 1200 km, which is on the order of the size of the photosphere itself. For a detailed study of the solar granulation and its relation to the hydrogen convection zone see Bray and Laughhead (1967).

Other evidence is the presence in the upper photosphere of the 300 sec oscillatory velocity field which presents a pattern of upward and downward vertical velocities on a scale somewhat larger than the granulation (Noyes, 1967; Bray and Laughhead, 1967). Although their complete physical nature is not fully understood, there seems to be little question of the existence of optically thick velocity fields.

b) Optically Thin Velocity Field Models

Most stellar investigations have used an isotropic and homogeneous (with depth) optically thin velocity fields for curve of growth studies. This "classical microturbulence" has also been employed in solar abundance investigations using the curve of growth method. In addition to classical microturbulence three other models of optically thin velocity fields have been studied. These models, shown in Figure 2, are most representative of the depth dependent models proposed in the last decade. They all have been obtained from analyses of solar line profiles.

The Utrecht model (Heintze, Hubenet and deJager, 1964) differs from the other depth dependent models in that it is isotropic. It decreases nearly linearly with depth. We have modified this model by allowing the velocity field to remain at an uniform maximum from $\log \tau_0 = -3.0$ to $\log \tau_0 = -4.0$. This extension was done for computational simplicity and is unimportant as all but the very strongest lines are formed well below this depth.

Both the Schmalberger (1963) and Gonczi and Roddier (1971) models have incorporated an anisotropy with the depth dependence. The tangential component is larger than the radial component to explain the broadening of solar lines as we look toward the limb. The Schmalberger model was also used with an extension to $\log \tau_0 = -4.0$ for the same reason as above. As the model proposed by Gonczi and Roddier (1971) was published for a two stream solar model an average of their values was employed in this study.

THIS BOOK CONTAINS NUMEROUS PAGES THAT WERE BOUND WITHOUT PAGE NUMBERS.

THIS IS AS RECEIVED FROM CUSTOMER.

Explanation of Plate I

Fig. 2. Depth dependent optically thin velocity fields (microturbulence) used in this study. The tangential and radial components are ξ_t and ξ_r respectively.

Fig. 3. Area velocity spectra which show the relative number of elements a_i in area A which have a velocity v. This spectrum is drawn for a scale velocity of 1 km/sec.

PLATE I

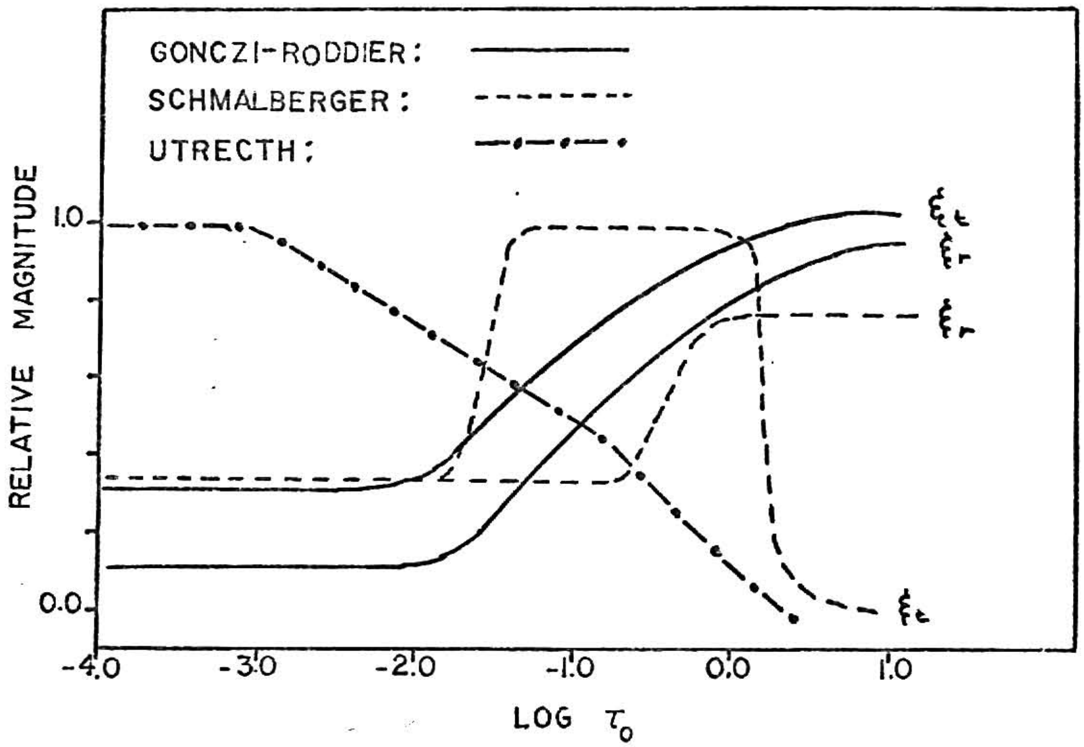
GONCZI-RODDIER:
SCHMALBERGER:
UTRECTH:
RELATIVE MAGNITUDE
1.0
0.0
ξ_t
ξ_r
ξ_r
ξ_t
-4.0
-3.0
-2.0
-1.0
0.0
1.0
LOG τ_0

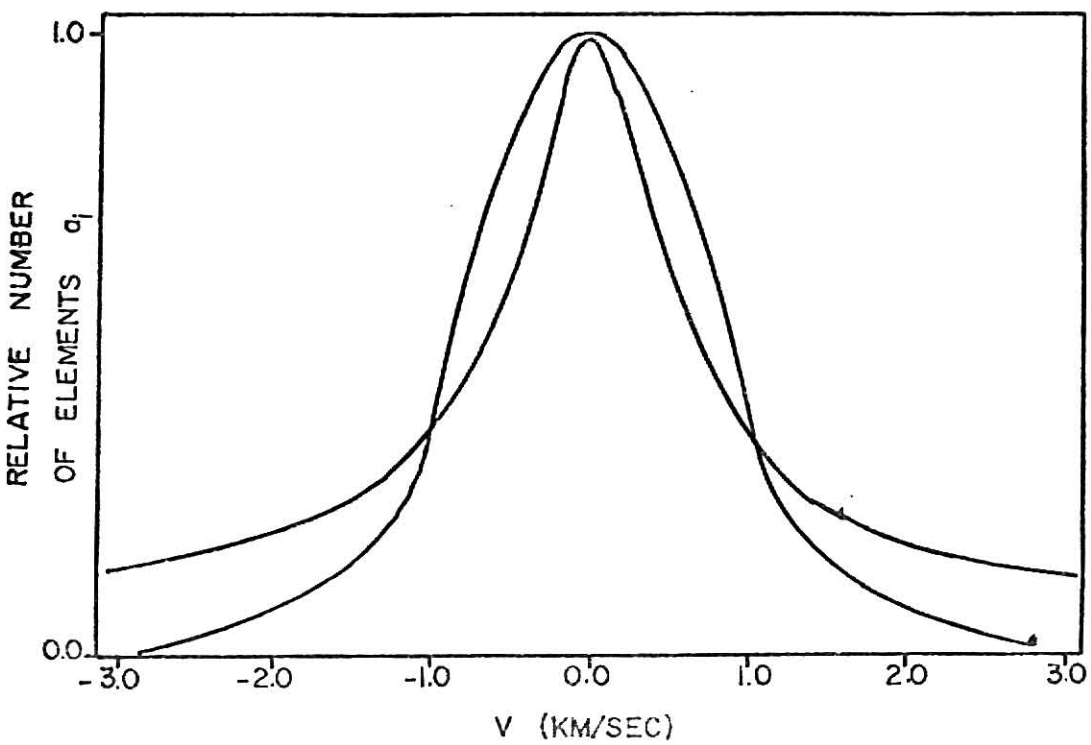
RELATIVE NUMBER OF ELEMENTS a_i
1.0
0.0
-3.0
-2.0
-1.0
0.0
1.0
2.0
3.0
V (KM/SEC)

All models are normalized to a maximum value of one, that is the maximum velocity is set equal to one and the remaining velocities are scaled as a fraction of that maximum. The values of the optically thin velocity fields used in this study are a multiple of these distributions.

It is felt that the four models discussed represent a good cross-section of possible distributions. Indeed, if a real distribution exists, one of the above models will be a good approximation.

c) Optically Thick Velocity Field Models

There is certainly not much precedent for the optically thick models, especially depth dependent ones. The most elementary case would be a random distribution of velocities which are isotropic and depth independent. There is, however, no a'priori reason to believe that large scale motions in a stellar atmosphere have these properties. If these large scale motions are transporting energy in some manner, as in convection, one may expect the motion to be preferentially radial, but the velocity distribution could still be almost anything. Also the energy transported by these motions is likely to be deposited in the low or high chromosphere so that optically thick velocity fields may also have some depth dependence. Under these conditions no choice of models is completely satisfactory. The models used are specified by the variation of the amplitude of velocity in both the radial and tangential components with optical depth.

The amplitudes are all relative to a scale velocity. The scale velocity is defined as the 1/e-width of the area-velocity distribution. The area-velocity distribution, as distinct from the depth dependence of velocity, specifies the relative number of area elements a_i of area A (see Chapter II) which are moving with a velocity v_i .

The choice of a velocity distribution is a vexing problem as the dynamical mechanism which give rise to large scale velocity fields are not completely defined. A random or Gaussian distribution was chosen for one trial. If we consider a velocity-area spectrum which is broader and does not decay as rapidly, then a triangular or a dispersion distribution would be reasonable.

In this study both Gaussian and dispersion distributions of velocity have been used. Figure 3 shows the velocity spectrum where the ordinate gives the number of area elements, a_i, which have velocity v_i. All velocities are in units of the scale velocity which was taken at the 1/e -width of the distribution. The number of area elements, η , used was a function of the scale velocity, S, as follows:

if $0.0 < S \leq 1.00$ then $\eta = 15$;

if $1.0 < S \leq 4.00$ then $\eta = 21$;

if $4.0 < S \leq 7.00$ then $\eta = 31$; and

if $S \geq 7.00$ then $\eta = 41$.

The above values of η were determined such that the resulting profile was reasonably smooth, that is no doppler components could be resolved.

Beckers and Morrison (1970) have published measurements of doppler velocities in a granual for both the radial and tangential directions. These velocities are for the top of a granulation cell which is generally believed to be at an optical depth on the order of unity (deJager and Neven, 1968). deJager and Neven (1967) contend that convective motions may persist up to optical depths on the order of $\tau_0 \sim 0.1$ ($\log \tau_0 = -1.00$) by an overshooting mechanism. The above leads us to propose a model where the radial velocity remains at an uniform maximum to optical depth unity and then linearly decays to zero at optical depth 0.1. The tangential velocity is about one-half the tangential velocity, as per Beckers and Morrisons measurements, and decays outward similarily to the radial. We have also incorporated a decay inward for the tangential component (see Figure 4) from a maximum at optical depth unity. This is based on the assumption that deep in the atmosphere the motion is due primarily to connection and is radial.

The other models used in this study are more hypothetical. However, it is felt that they are reasonable trials in view of the lack of definitive observations. An anisotropic-homogeneous model was used based on the idea that the mechanism giving rise to the velocity field has a preferential direction. For this model the radial component is twice the tangential component. Here we are again using the granulation and its relation to convection as a basis.

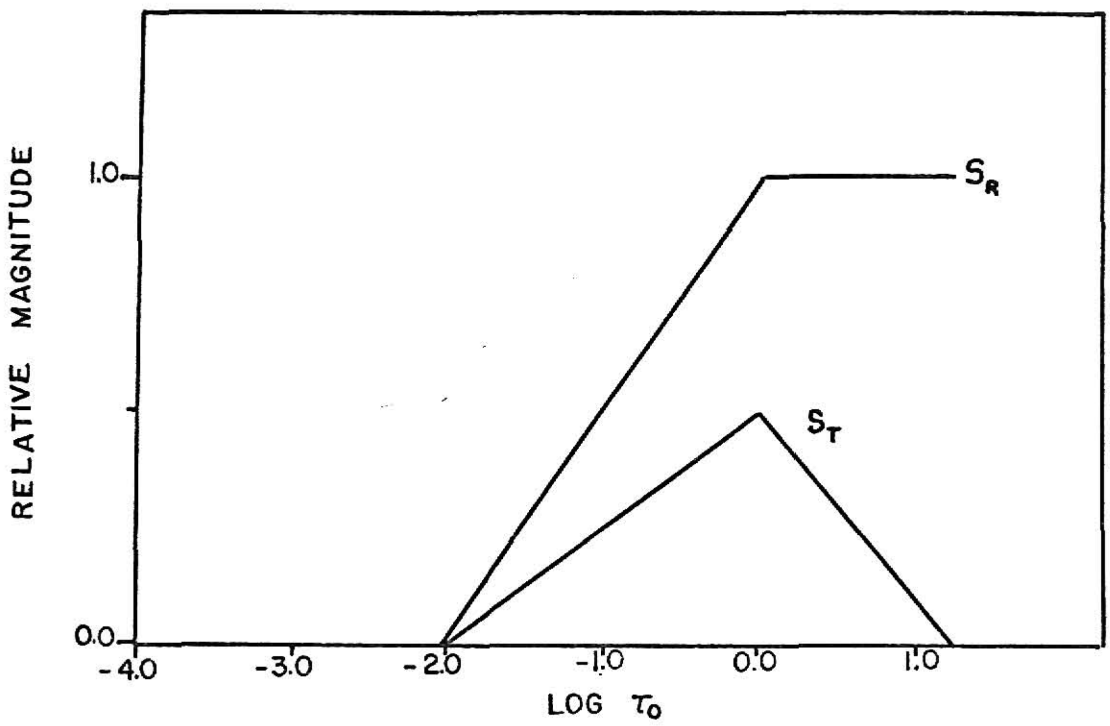

Fig. 4 - Variation of the semi-empirical optically thick velocity field model with depth where the radial and tangential components are S_r and S_t respectively.

This model may be more realistic for stars of earlier spectral type than the sun as the importance of convection increases till about F5V. In the atmospheres of these stars one might expect optically thick velocity fields to play a major role in shaping the line profiles.

An isotropic-homogeneous model where both radial and tangential components are equal, this model may be more likely to approximate conditions in the atmospheres of early type stars where there is little or no convection.

It should be emphasized that none of the above models of optically thick velocity fields are meant to detail the physical state of the solar (or stellar) atmosphere or model the solar granules. It is the main purpose of this study to ascertain qualitative effects on line profiles by varying the model parameter. Although many more models are possible, and indeed feasible, the above are sufficient to gain some insight into the effect of optically thick velocity fields on line profiles.

IV. NUMERICAL RESULTS FOR THE VARIOUS MODELS ON SOLAR INTENSITY LINE SHAPES

a) Curve of Line Shape Diagram

It is desirable to express the shape of an absorption line in terms of parameters which can be readily measured for a large number of lines in a spectrum. The inaccuracies of standard photographic spectrophotometry precludes in most cases an actual plot of the measured profile. The curve of line shape diagram (Elste, 1967) plots the equivalent width on the abscissa and the ratio of the 3/4 width to the 1/2 width on the ordinate. Such a plot was hinted at before by Slettebak (1956). The above ratio is a quantitative measure of the sharpness or triangularity of a line. For a U-shaped or rectangular line, the ratio will approach unity as a limit and for a V-shaped line, the ratio will approach one-half. For a very strong line with a well developed wings, this ratio can become smaller than one-half.

To start with, consider an absorption line with no broadening by velocity fields which is described by a Voigt function. By increasing the number of absorbing atoms in the line of sight, the profile area grows as resulting in the curve of growth (Mihalas, 1970; Cowley, 1970). By calculating the equivalent widths of the line for different numbers of absorbing atoms or ions, we can generate a theoretical curve of growth (see Appendix A). Let us now see how the ratio of the 3/4 width, t, to the 1/2 width, h, develops as we move along the curve of growth. For weak lines which are on the linear portion, the profiles are essentially Gaussian due to the dominance of the thermal broadening on the line absorption coefficient. The central depth is increased more or less in proportion to the half-width. Similarly, the ratio of 3/4 width to 1/2 width, t/h, remains more or less constant. As we approach optical saturation, however, the line width grows much faster than the central depth. The damping wings have not yet begun to develop and the increase in equivalent width occurs in the Doppler core. Thus the ratio, t/h, begins to increase relative to the equivalent width. As we move along the flat portion of the curve of growth, the line reaches its maximum central depth and continues to saturate at wavelengths near the line center with only a slight development of wings. At this point, the ratio, t/h, will rapidly approach a maximum value. Moving along into the damping region of the curve of growth, the wings rapidly develop and the half-width increases while the 3/4-width remains nearly constant. Eventually the 3/4 width grows relative to the 1/2 width and the ratio, t/h, falls off sharply to lower values as is shown in Figure 5. We will now proceed to analyze what effect velocity fields of both small and large scale have on the development of the ratio, t/h, for the same increase in the number of absorbing atoms.

It is felt by the writer that the curve of line shape diagram, or some similar analysis, is necessary to differentiate the

Explanation of Plate II

Fig. 5. Comparison of curve of growth (upper) and curve of line shape (lower) for FeI (1) λ 5250 with no velocity fields. Note that the curve of growth is drawn with the axes reversed from normal.

PLATE II

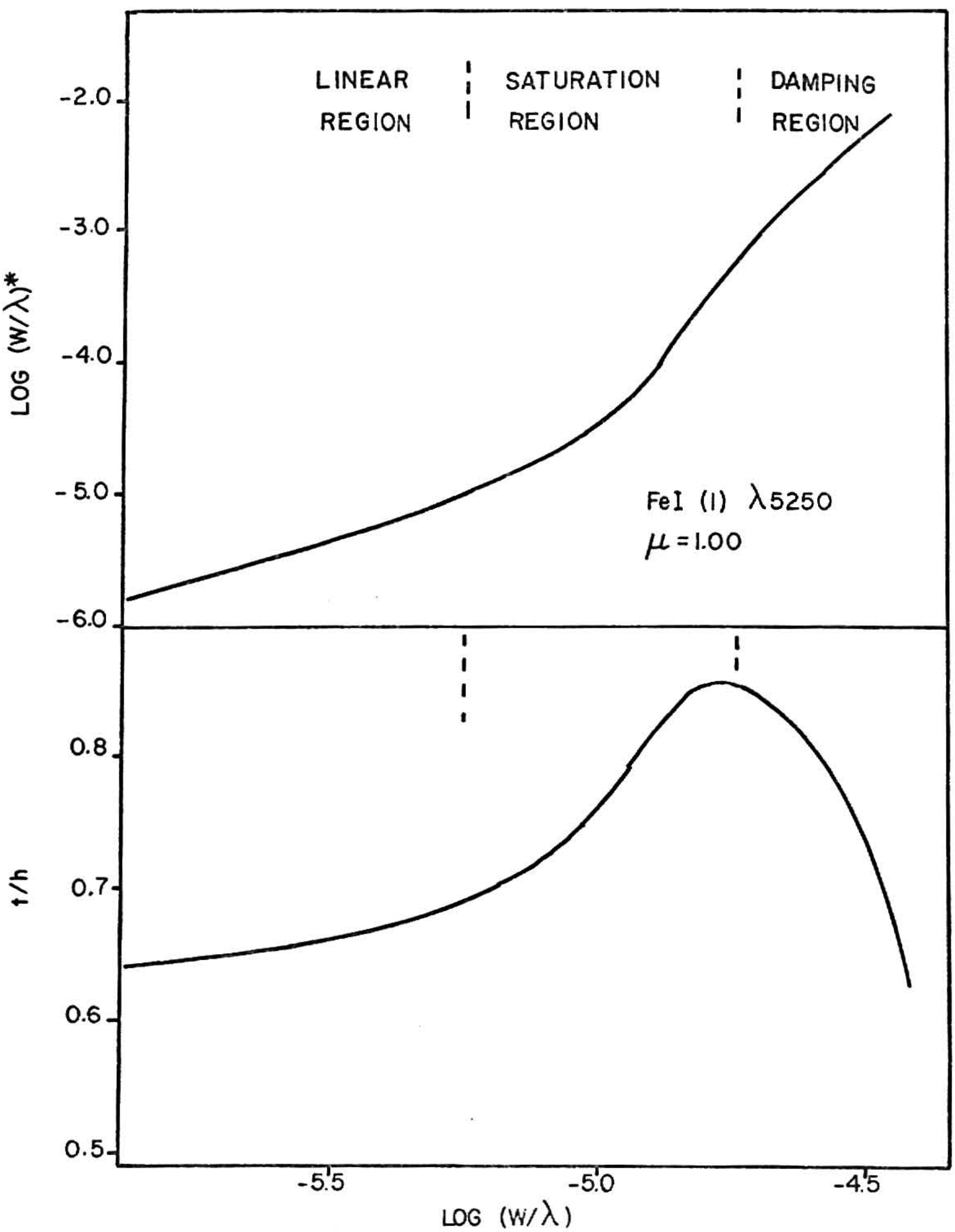
LINEAR REGION
SATURATION REGION
DAMPING REGION
-2.0
-3.0
-4.0
-5.0
-6.0
LOG (W/λ)*
FeI (1) λ5250
μ = 1.00
0.8
0.7
0.6
0.5
t/h
-5.5
-5.0
-4.5
LOG (W/λ)

effects of optically thin velocity fields and optically thick velocity fields. Although this can supposedly be done using a curve of line width (Huang and Struve, 1952; van den Heuvel, 1963), the results are ambiguous with all but the very best data. Half widths were measured for calculated line profiles using the same values of velocity for both optically thin and optically thick velocity fields. These measurements are displayed in Figure 6 with the logrithm of the equivalent width divided by the wavelength on the abscissa and the logrithm of the 1/2-width divided by the wavelength on the ordinate. This theoretical curve of line width demonstrates that the qualitative effect can be quite similar.

b) Optically Thin Velocity Fields

As discussed in Section III, the optically thin velocity fields are essentially microturbulence. Curves of line shape were calculated for all the models described in Section III for the center of the disk. The basic qualitative behavior of all the models is the same and only the classical microturbulence, isotropic-depth independent, will be discussed for calculation at the center of the disk, $\mu = 1.0$.

Figure 7 shows the effect of increasing optically thin velocity field on the theoretical curve of growth of the line FeI (1) λ 5250.21. As it is well known, the increasing velocity of the velocity field delays the onset of saturation; thereby raising

Explanation of Plate III

Fig. 6. Curve of line width for FeI (1) λ 5250 showing the effect of both optically thick and optically thin velocity fields.

Fig. 7. Curve of growth for FeI (1) λ 5250 showing the effect of optically thin velocity fields (classical microturbulence).

PLATE III

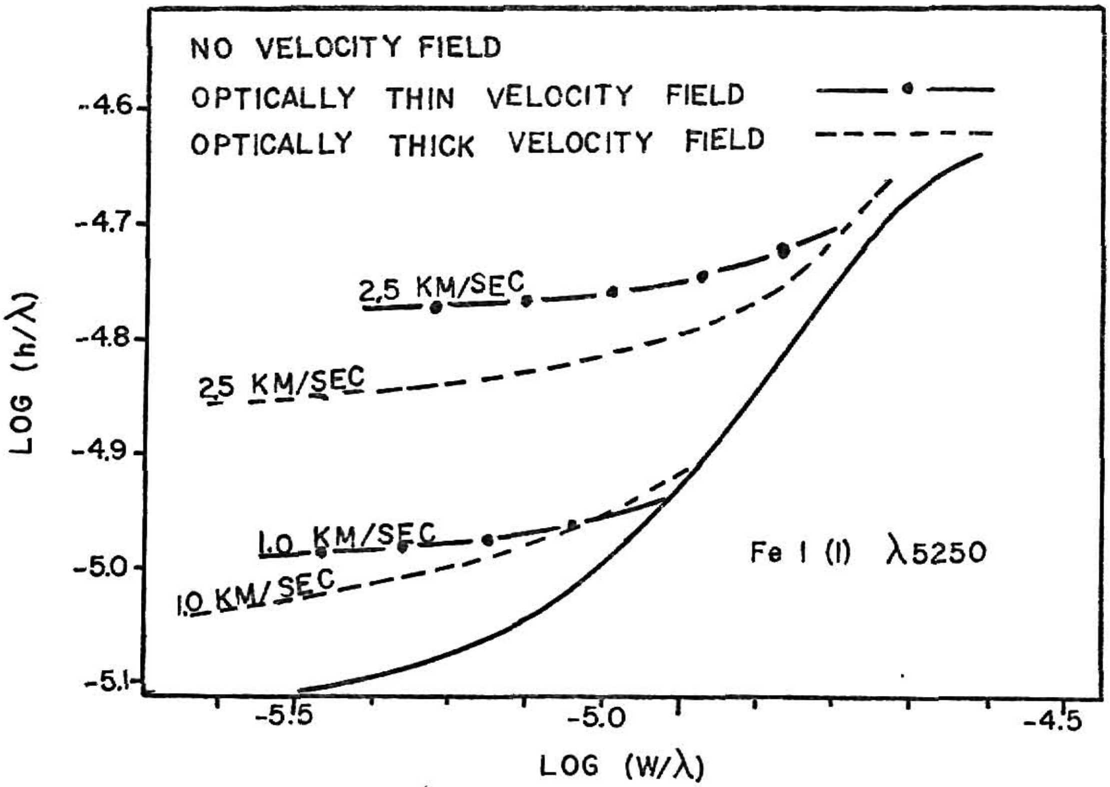
NO VELOCITY FIELD
OPTICALLY THIN VELOCITY FIELD
OPTICALLY THICK VELOCITY FIELD
2.5 KM/SEC
2.5 KM/SEC
1.0 KM/SEC
1.0 KM/SEC
Fe I (1) λ5250
LOG (h/λ)
-4.6
-4.7
-4.8
-4.9
-5.0
-5.1
-5.5
-5.0
-4.5
LOG (W/λ)

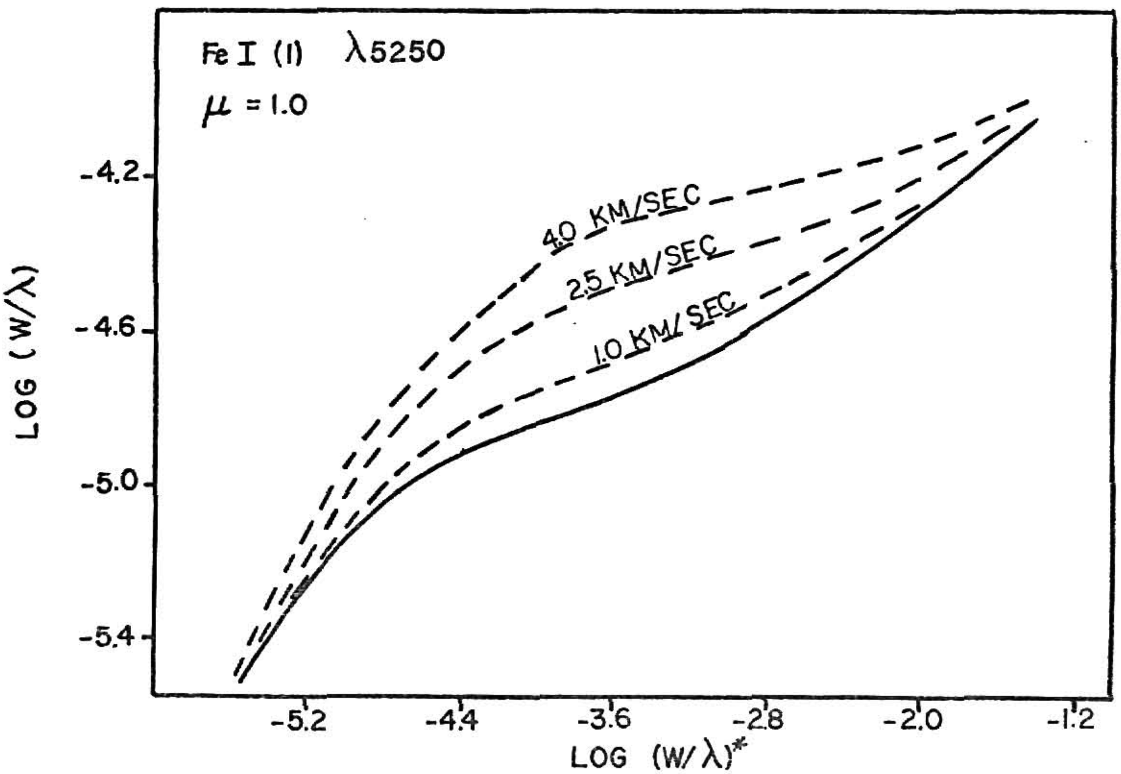
Fe I (1) λ5250
μ = 1.0
4.0 KM/SEC
2.5 KM/SEC
1.0 KM/SEC
LOG (W/λ)
-4.2
-4.6
-5.0
-5.4
-5.2
-4.4
-3.6
-2.8
-2.0
-1.2
LOG (W/λ)*

the flat portion of the curve of growth. The effect of this increasing velocity field on the curve of line shape can be understood in terms of its effect on the curve of growth. Increasing microturbulence causes the peak, which occurs at the same values of equivalent widths as the saturation region in the corresponding curve of growth, to shift toward larger equivalent widths. Also the peaks in the curve of line shape increase in magnitude as the value of the velocity field increases. This indicates an increase in the U-shape of the line profile which is characteristic of increasing microturbulence. Figure 8 shows the curves of line shape for the FeI (1) λ 5250.21 line for the same velocities displayed in Figure 7. Figure 9 shows a similar plot for a higher excitation line, FeI (687) λ 4863.24. The qualitative behavior of both the low and high excitation lines is identical. It is useful to look at the line profiles themselves for increasing optically thin velocity fields. Figure 10 displays computed profiles as affected by increasing velocity for weak, medium, and strong lines. Particularly note that for the medium and strong lines the control depth changes very little as the profile widens.

Calculations at a limb distance of μ = 0.4 show a similar behavior as center of the disk calculations for both the classical microturbulence and the Utrecht model (Figure 11). Schmalberger's inhomogeneous anisotropic model, however, behaves somewhat differently as large velocities tend to triangulate the lines (Figure 12).

Explanation of Plate IV

Fig. 8. Curve of line shape for FeI (1) λ 5250 for several values of classical microturbulence at μ = 1.0. The zero velocity curve is also shown.

Fig. 9. Curve of line shape as in Fig. 8 except for FeI (687) λ 4863.

PLATE IV

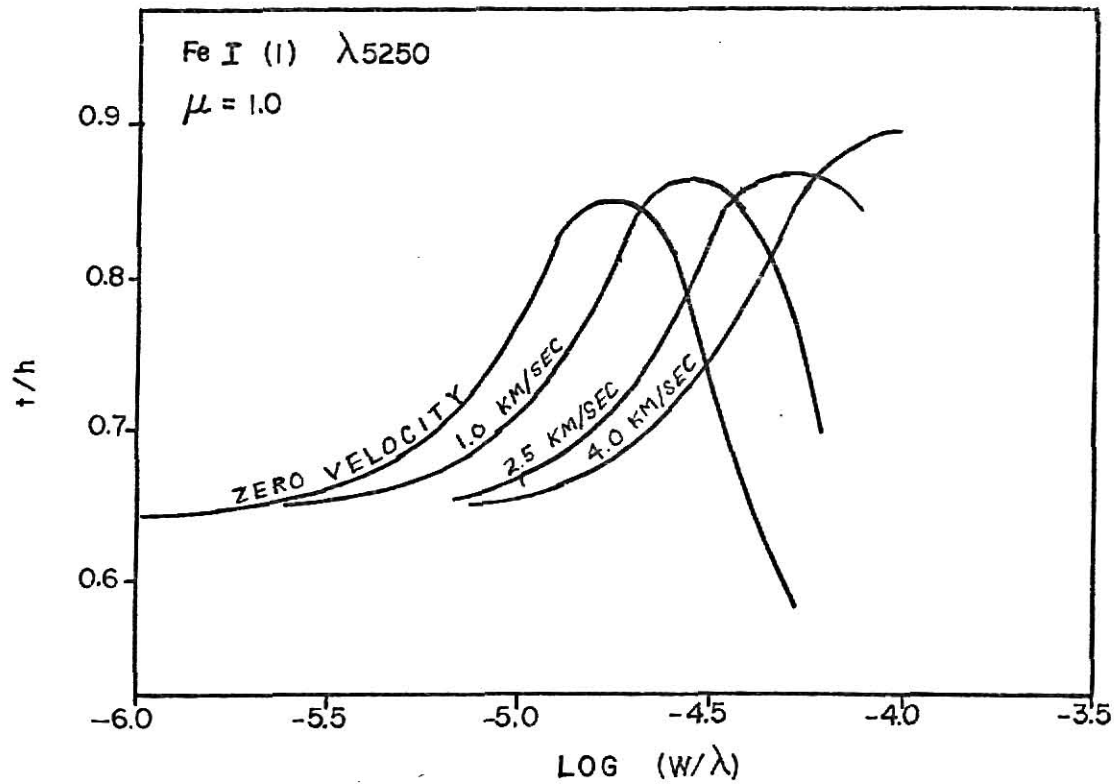
Fe I (1) λ5250
μ = 1.0
0.9
0.8
0.7
0.6
t/h
ZERO VELOCITY
1.0 KM/SEC
2.5 KM/SEC
4.0 KM/SEC
-6.0
-5.5
-5.0
-4.5
-4.0
-3.5
LOG (W/λ)

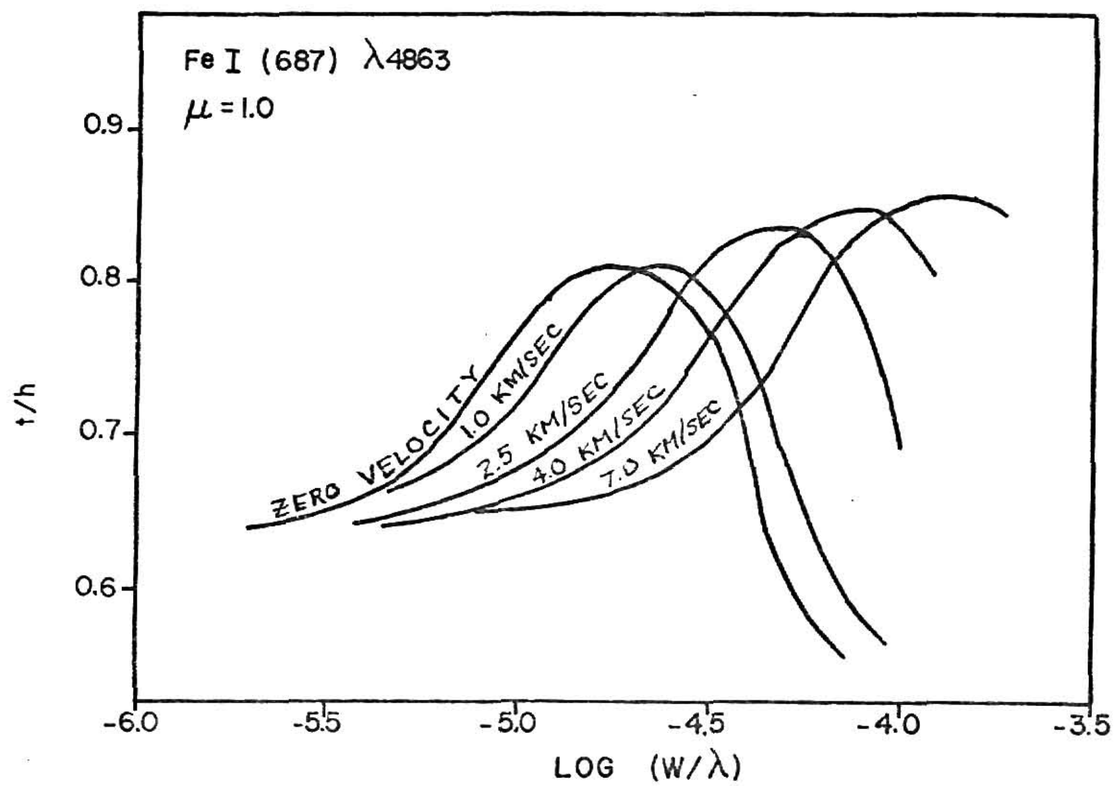
Fe I (687) λ4863
μ = 1.0
0.9
0.8
0.7
0.6
t/h
ZERO VELOCITY
1.0 KM/SEC
2.5 KM/SEC
4.0 KM/SEC
7.0 KM/SEC
-6.0
-5.5
-5.0
-4.5
-4.0
-3.5
LOG (W/λ)

Explanation of Plate V

Fig. 10. Line profiles of FeI (687) λ 4862 for increasing velocities in an optically thin velocity field. From left to right are weak, medium, and strong lines which were computed using abundances of $\log \epsilon = -5.8, -4.5$, and -3.7, respectively. Calculations were done at $\mu = 1.0$.

PLATE V

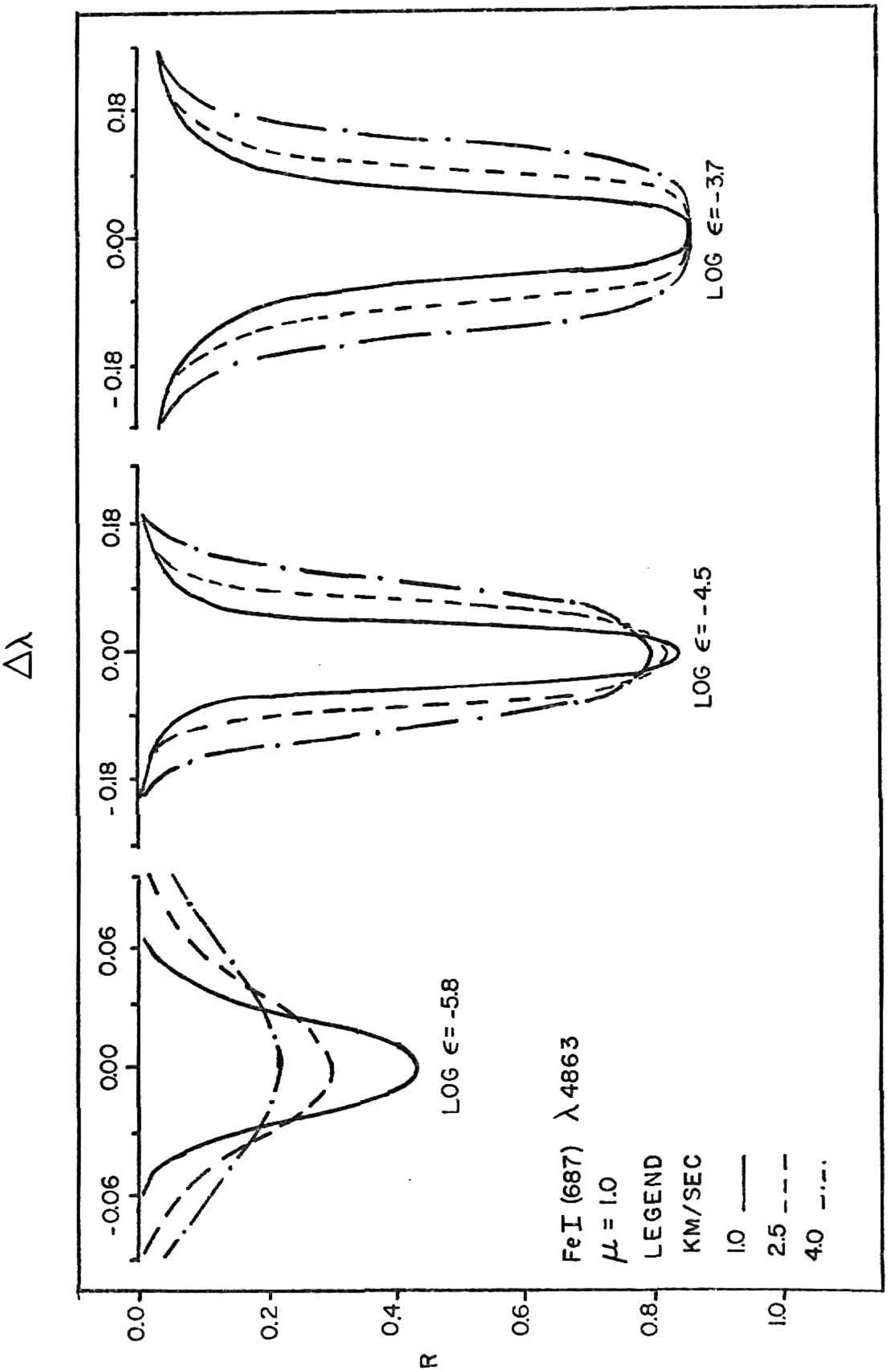

Δλ
-0.06
0.00
0.06
-0.18
0.00
0.18
-0.18
0.00
0.18
LOG ∈= -5.8
LOG ∈= -4.5
LOG ∈= -3.7
Fe I (687) λ 4863
μ = 1.0
LEGEND
KM/SEC
1.0
2.5
4.0
0.0
0.2
0.4
0.6
0.8
1.0
R

Explanation of Plate VI

Fig. 11. Curve of line shape for FeI (1) λ 5250 at $\mu = 0.4$ for the Utrecht optically thin velocity field model.

Fig. 12. Curve of line shape for FeI (1) λ 5250 at $\mu = 0.4$ for the Schmalberger distribution of an optically thin velocity field.

PLATE VI

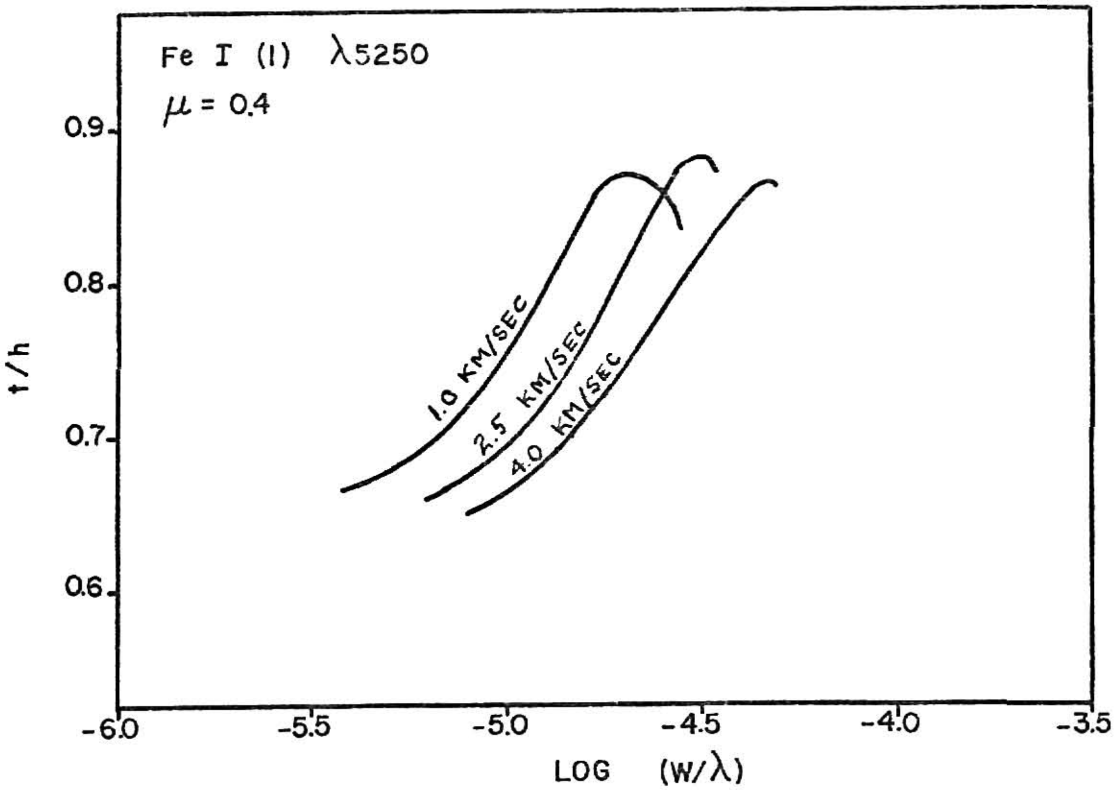
Fe I (1) λ5250
μ = 0.4
0.9
0.8
0.7
0.6
t/h
1.0 KM/SEC
2.5 KM/SEC
4.0 KM/SEC
-6.0
-5.5
-5.0
-4.5
-4.0
-3.5
LOG (W/λ)

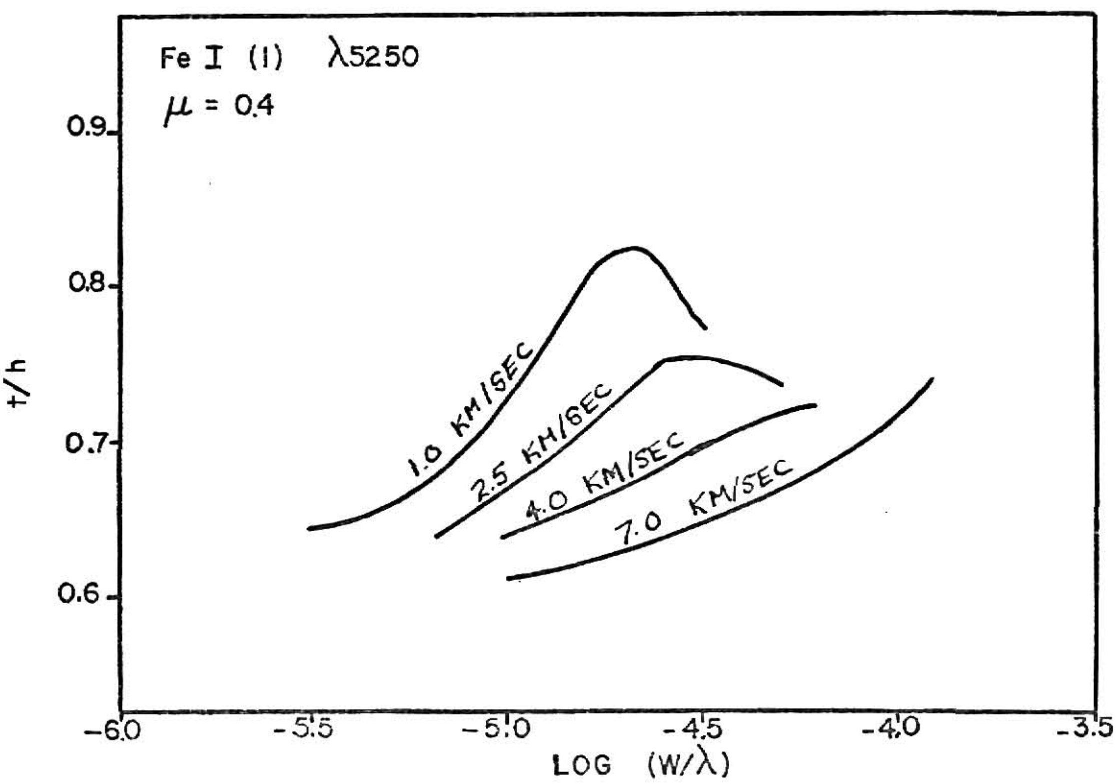
Fe I (1) λ5250
μ = 0.4
0.9
0.8
0.7
0.6
t/h
1.0 KM/SEC
2.5 KM/SEC
4.0 KM/SEC
7.0 KM/SEC
-6.0
-5.5
-5.0
-4.5
-4.0
-3.5
LOG (W/λ)

The velocities of the optically thin velocity fields, which do begin to triangulate the lines appreciably, are near sonic velocities in the solar photosphere. Sonic velocities here are on the order of 7 km/sec.

c) Optically Thick Velocity Fields

As the optically thick velocity fields do not significantly effect the line equivalent width, it will not alter the curve of growth. However, these velocity fields do manifest themselves in the curve of line shape diagram in a rather dramatic way. Let us first consider an isotropic, homogeneous model with a Gaussian distribution of velocities, IHG model. As Figure 13 reveals, the peak in the curve of line shape shrinks with increasing velocity, i.e., the lines incline to become more triangular as the velocity increases. Furthermore, it is of significance that the peak drops extremely rapidly and is all but gone with a scale velocity of only 2.5 km/sec. Figure 14 shows the calculations for an isotropic, homogeneous model with a dispersion distribution, IHD model. The weak lines are more triangular with this model, but the qualitative trend is identical to the IHG model. This tendency is independent of the velocity distribution used. This is pleasing since there are really no strong physical arguments for the chosen velocity distributions. The small quantitative differences are too small to be detectable and even if they could be measured we have no guarantee that a particular curve of line shape is unique to one velocity distribution.

Explanation of Plate VII

Fig. 13. Curve of line shape for FeI (1) λ 5250 showing the effect of an optically thick, isotropic, homogeneous velocity field with a Gaussian distribution at $\mu = 1.0$.

Fig. 14. Curve of line shape as in Fig. 13 except velocity field has a dispersion area-velocity distribution.

PLATE VII

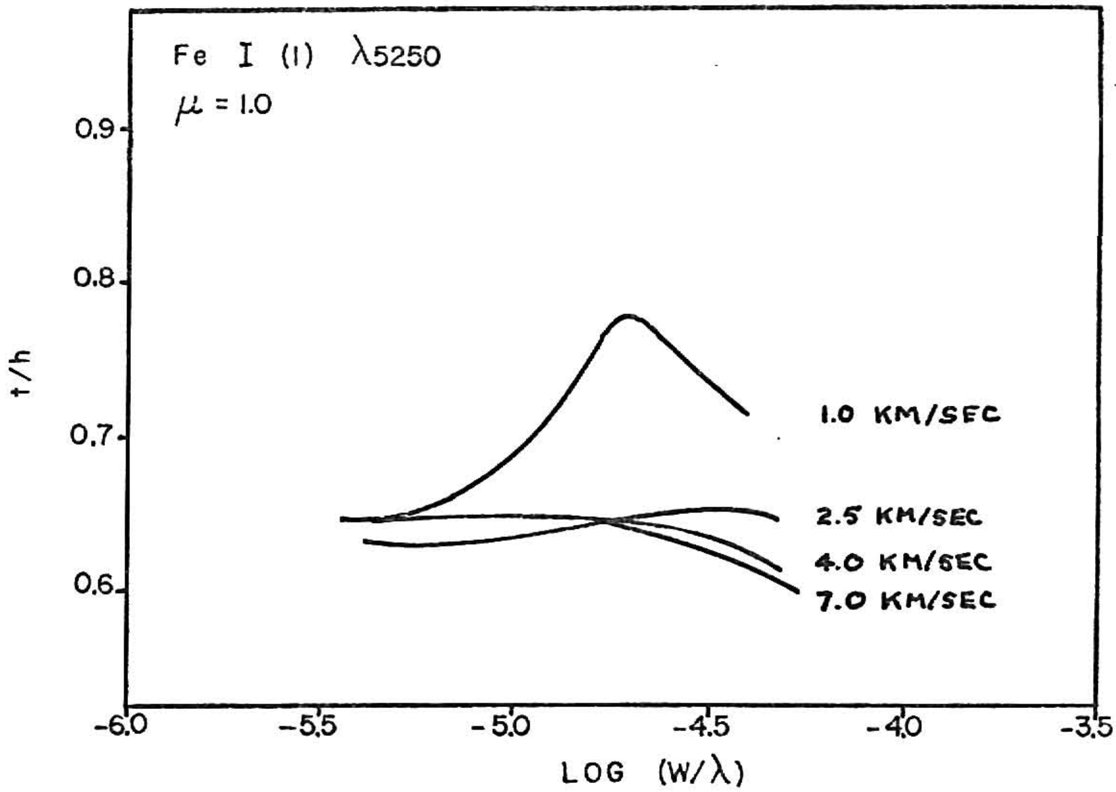
Fe I (1) λ5250
μ = 1.0
0.9
0.8
0.7
0.6
t/h
1.0 KM/SEC
2.5 KM/SEC
4.0 KM/SEC
7.0 KM/SEC
-6.0
-5.5
-5.0
-4.5
-4.0
-3.5
LOG (W/λ)

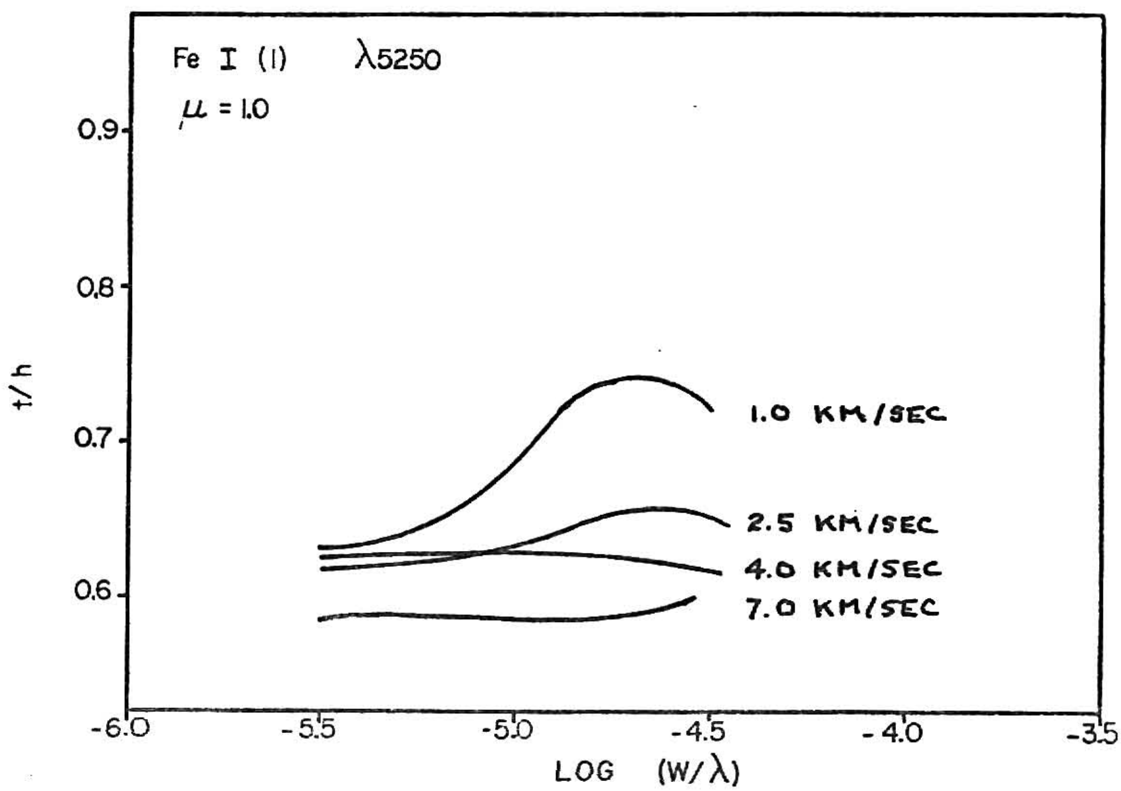
Fe I (1) λ5250
μ = 1.0
0.9
0.8
0.7
0.6
t/h
1.0 KM/SEC
2.5 KM/SEC
4.0 KM/SEC
7.0 KM/SEC
-6.0
-5.5
-5.0
-4.5
-4.0
-3.5
LOG (W/λ)

To ascertain any differences in the isotropic and anisotropic models, calculations were made at limb distances $\mu = 0.4$. Figures 15 and 16 show these results. For both the isotropic and anisotropic models the presence of the tangential component has served to increase the line-of-sight velocity thereby triangulating the lines at even smaller velocities. The curve of line shape alone is too insensitive to distinguish between these models as far as velocity components are concerned. The saturation curve, which is a plot of line central depth vs. line equivalent width, is a great deal more sensitive to the line-of-sight velocity, and thus would be a more useful tool in determining the degree of anisotrophy where measurements are available at several limb distances as in the sun.

The semi-empirical model discussed in Section III has the same effect on the curve of line shape, but due to the small values of velocity in the line formation region, much larger velocities are needed in order to flatten the peak.

Line profiles calculated with an optically thick velocity field behave quite differently than those calculated in an optically thin field. Figure 17 shows the same lines as Figure 10, calculated using the optically thick velocity fields. One notices that in all cases increasing velocity decreases the central depth and increasing the amount of the equivalent width which appears in the wings. this is, of course, what causes the ratio t/h to decrease and give the line a more triangular appearance. Comparison of Figure 17 with Figure 10 indicates the qualitative difference in the effects of the optically thin and optically thick velocity fields.

Explanation of Plate VIII

Fig. 15. Curve of line shape for FeI (1) λ 5250 at μ = 0.4 using an isotropic optically thick velocity field with a Gaussian distribution.

Fig. 16. Same as Fig. 15 except an anisotropic optically thick velocity field model is used.

PLATE VIII

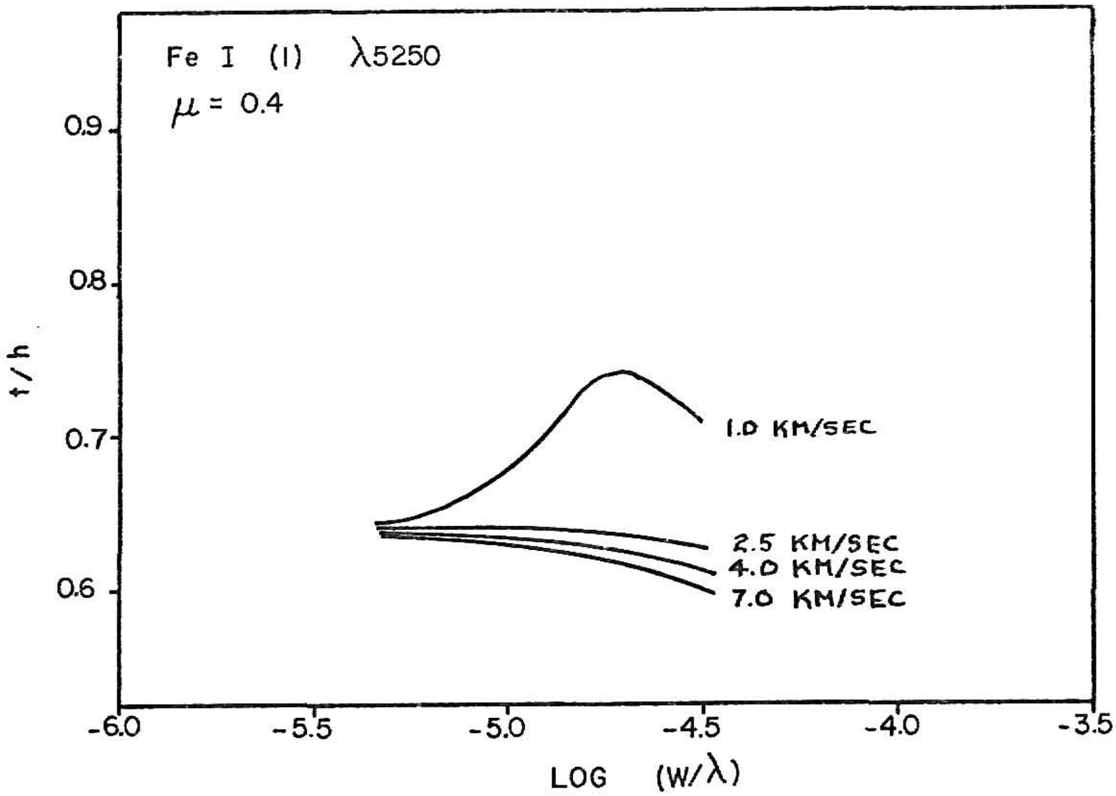
Fe I (1) λ5250
μ = 0.4
0.9
0.8
0.7
0.6
t/h
1.0 KM/SEC
2.5 KM/SEC
4.0 KM/SEC
7.0 KM/SEC
-6.0
-5.5
-5.0
-4.5
-4.0
-3.5
LOG (W/λ)

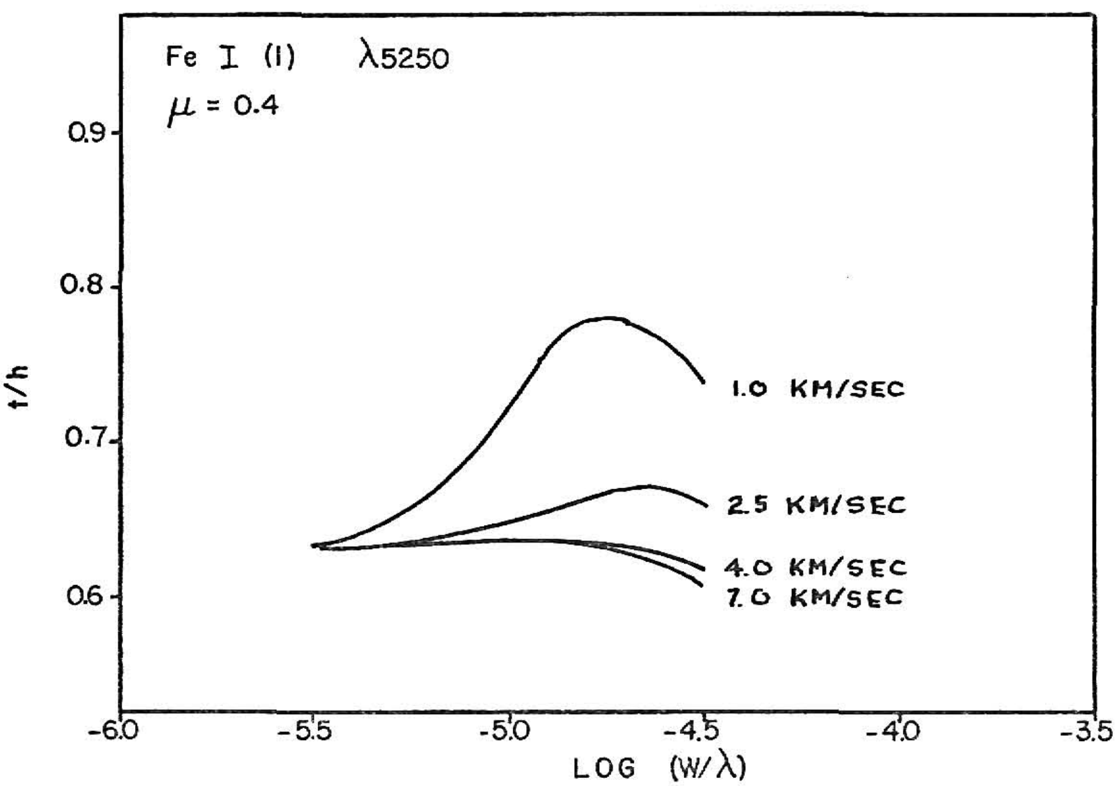
Fe I (1) λ5250
μ = 0.4
0.9
0.8
0.7
0.6
t/h
1.0 KM/SEC
2.5 KM/SEC
4.0 KM/SEC
7.0 KM/SEC
-6.0
-5.5
-5.0
-4.5
-4.0
-3.5
LOG (W/λ)

Explanation of Plate IX

Fig. 17. Same as Fig. 10 except for an optically thick velocity field model. It should be noted that the profiles in this figure, except for the weak line, are markedly different than those in Figure 10.

PLATE IX

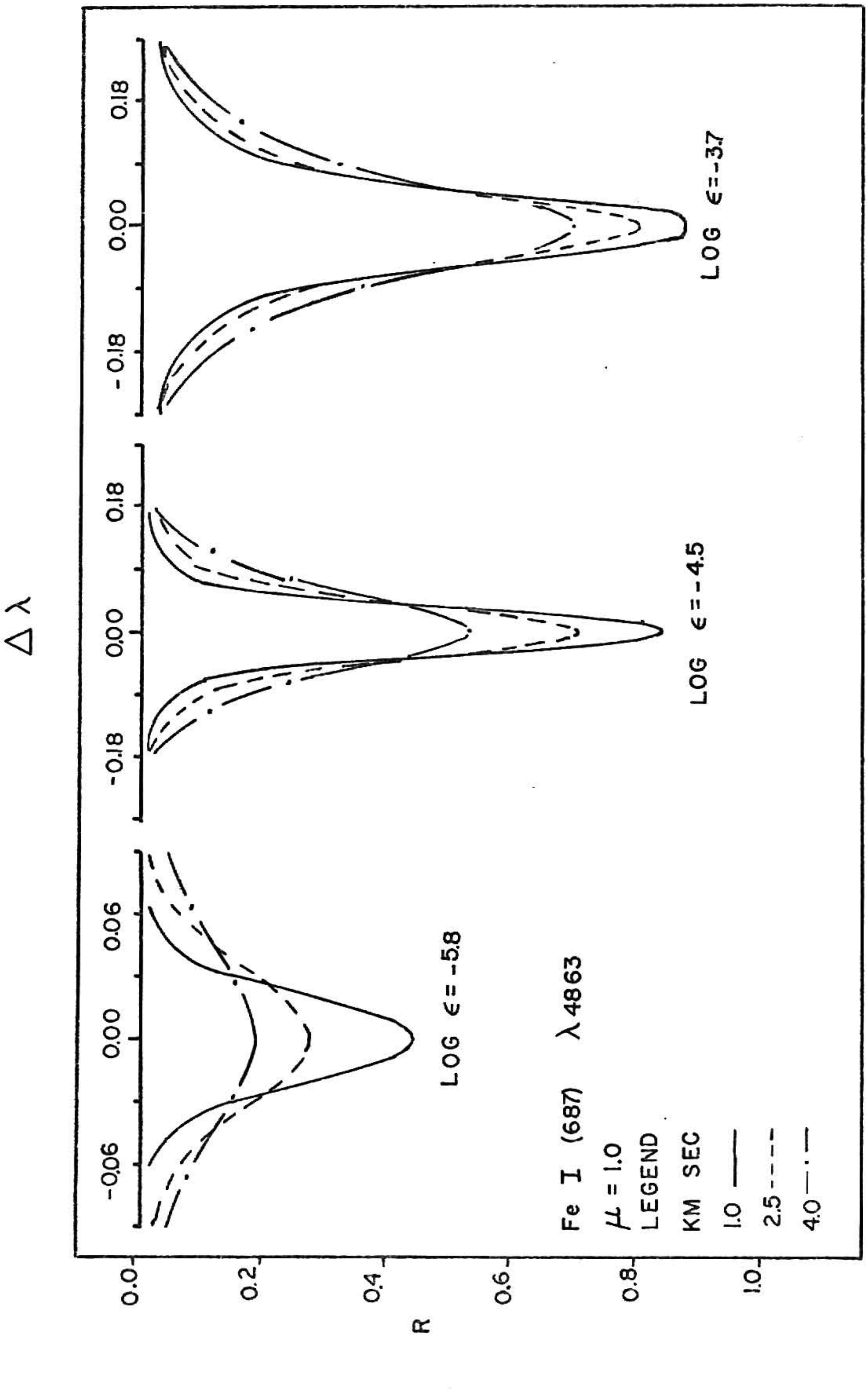

Δλ
-0.18
0.00
0.18
LOG ε = -3.7
LOG ε = -4.5
-0.06
0.06
LOG ε = -5.8
λ 4863
Fe I (687)
μ = 1.0
LEGEND
KM SEC
1.0
2.5
4.0
0.0
0.2
0.4
0.6
0.8
1.0
R

V. RESULTS FOR FLUX LINE SHAPES

If we use the analytical formulations for flux line depth (Aller, 1963; Cowley, 1970), we are restricted to optically thin velocity fields which are isotropic and optically thick velocity fields whose line-of-sight components are constant across the disk. These would be an unrealistic set of assumptions. Since the emergent flux from a star is defined as the integrated intensity over the surface, we can express flux as a numerical integration of intensity over the stellar disk. The flux profiles calculated in this study were obtained by numerically integrating four intensity profiles calculated at $\mu = 1.0, 0.7, 0.4$, and 0.2. When compared with an analytical flux calculation with no velocity fields, the numerical integration scheme is accurate to better than 1% over most of the profile. The same solar model used above was used in these calculations.

As there is no reason to expect the isotropic models of optically thin velocity fields to behave differently in flux than in intensity, only the Schmalberger model was tested. It is observed from Figure 18 that the curve-of-line shape resembles the behavior noticed in Figure 12, that is the triangulation of the profile with large velocity. The triangulation in flux, however, takes place at somewhat lower velocities. This is due to the increased importance of the tangential component which has a steep gradient in the line formation region. Although the velocities are still rather large for the sun, such a distribution of microturbulence cannot readily

Explanation of Plate X

Fig. 18. Curve of line shape in flux for FeI (687) λ 4863 using the Schmalberger distribution of an optically thin velocity field.

Fig. 19. Curve of line shape in flux for FeI (687) λ 4863 using an anisotropic, homogeneous optically thick velocity field model.

PLATE X

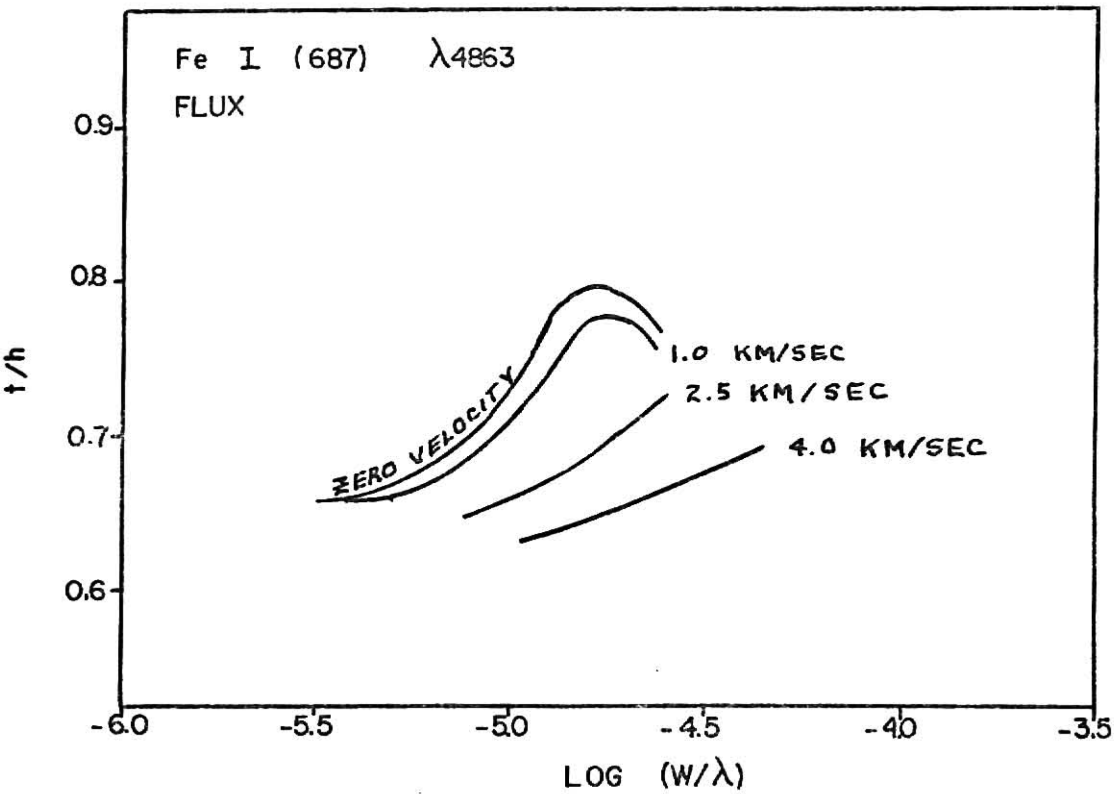
Fe I (687) λ4863
FLUX
0.9
0.8
0.7
0.6
t/h
ZERO VELOCITY
1.0 KM/SEC
2.5 KM/SEC
4.0 KM/SEC
-6.0
-5.5
-5.0
-4.5
-4.0
-3.5
LOG (W/λ)

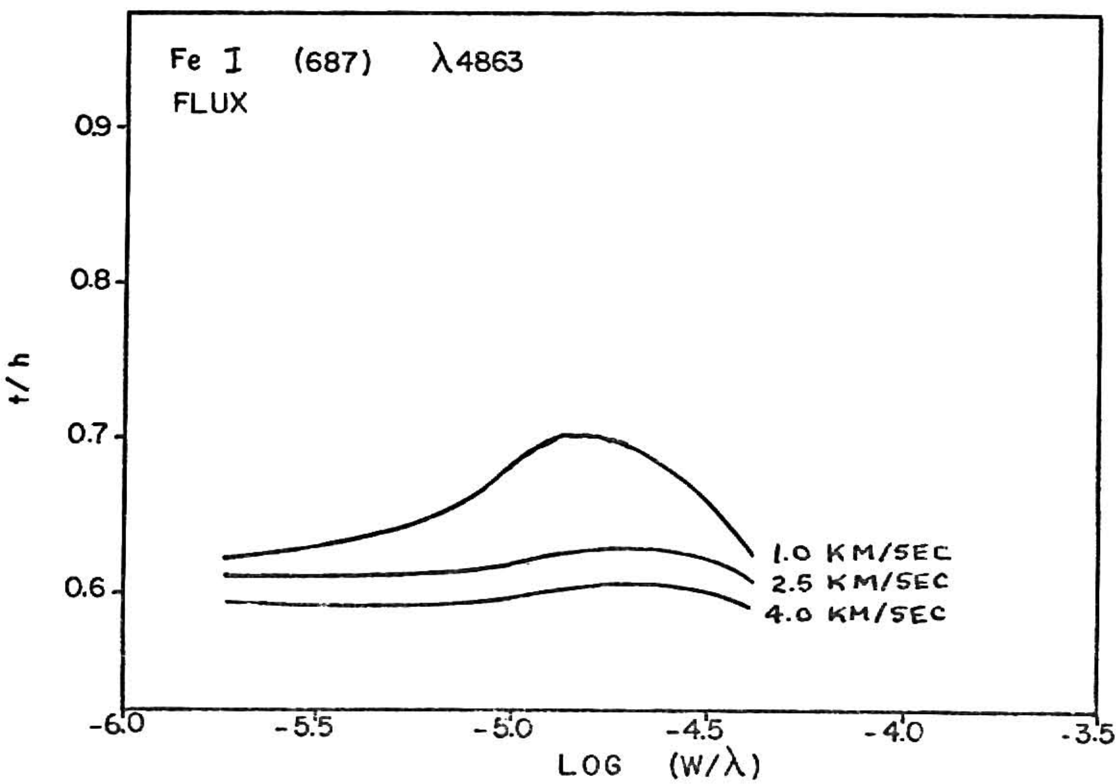
Fe I (687) λ4863
FLUX
0.9
0.8
0.7
0.6
t/h
1.0 KM/SEC
2.5 KM/SEC
4.0 KM/SEC
-6.0
-5.5
-5.0
-4.5
-4.0
-3.5
LOG (W/λ)

be dismissed as a way of triangulating line profiles and making the proposed distinction ambiguous.

Figure 19 displays the calculations for three scale velocities of an anisotropic, homogeneous, optically thick velocity field calculated with a Gaussian distribution. Again the behavior is almost identical to the results in Section IV as indicated by the curve-of-line shape diagram. As was the case for the previous calculations displayed in Figures 15 and 16, the peaks in the curve-of-line shape are depressed by the increase of the line-of-sight velocity at intermediate limb distances. Calculations were also done for the anisotropic model with a dispersion distribution and a isotropic model with a Gaussian distribution. As in Figure 19, these calculations yield results very similar to those in Section IV.

Even with excellent spectrophotometric data it would be almost impossible to sort out the detailed structure of the large scale velocity field in stars. The above diagrams only allow a distinction between scale of velocity field at best.

VI. CONCLUSIONS

We have shown in Section IV that the effects of optically thin and optically thick velocity fields on intensity line profiles are not readily distinguishable using the curve-of-line width (see Figure 6). In this same section, we have also shown that the optically thin and the optically thick velocity fields each have a characteristic effect on the curve-of-line shape which is independent to a large degree of the model employed and of the lines used for this study. In Section V, the results of Section IV were verified for flux line profiles.

Within the context of the models used in this investigation one can see that there is no qualitative or quantitative similarity between lines formed in optically thin and optically thick velocity fields when the magnitude of the motions is greater than 2 km/sec. This statement is true for lines which lie on the flat portion of the curve of growth. Most observed lines do fall in this region for both the sun and most other stars. Since weak lines reflect the shape of the line absorption coefficient, they cannot be used to distinguish the between the optically thick and thin velocity fields. The difference between the two types of velocity fields is perhaps best seen by contrasting the line profiles in Figure 10 with those in Figure 17.

If optically thin velocity fields, as discussed above, are significant in shaping spectral lines in the sun and other stars, as is often claimed, then an empirical curve-of-line shape should reflect this in some way. There is some evidence to the contrary as is shown in Figure 20 and in a study of solar lines by Elste (1967). Figure 20 is composed of data taken from a study by Hardop and Scholz (1970) of the BOV star Υ Scorpii. For Υ Scorpii the mean value of t/h is about 0.63 and the points define a reasonably flat line for all values of equivalent width. One may be able to say, at least, that classical microturbulence is not a dominate broadening mechanism. In the above mentioned study by Elste, the solar lines he analyzed also show a remarkably flat curve-of-line shape. Elste was also particularly careful to remove the instrumental profile. The above solar data and the results of this study support the view that optically thick velocity fields are an important if not dominant effect in shaping solar line profiles. One is also led to question the concept of microturbulence as presently accepted.

Before definite statements on the existence of small scale velocity fields and the importance of optically thick velocity fields can be made, more detailed models which more closely match the state of the solar photosphere will have to be constructed. Also needed are high quality observations, especially of stars, so the actual observed line profiles can be used to test the validity of the theory.

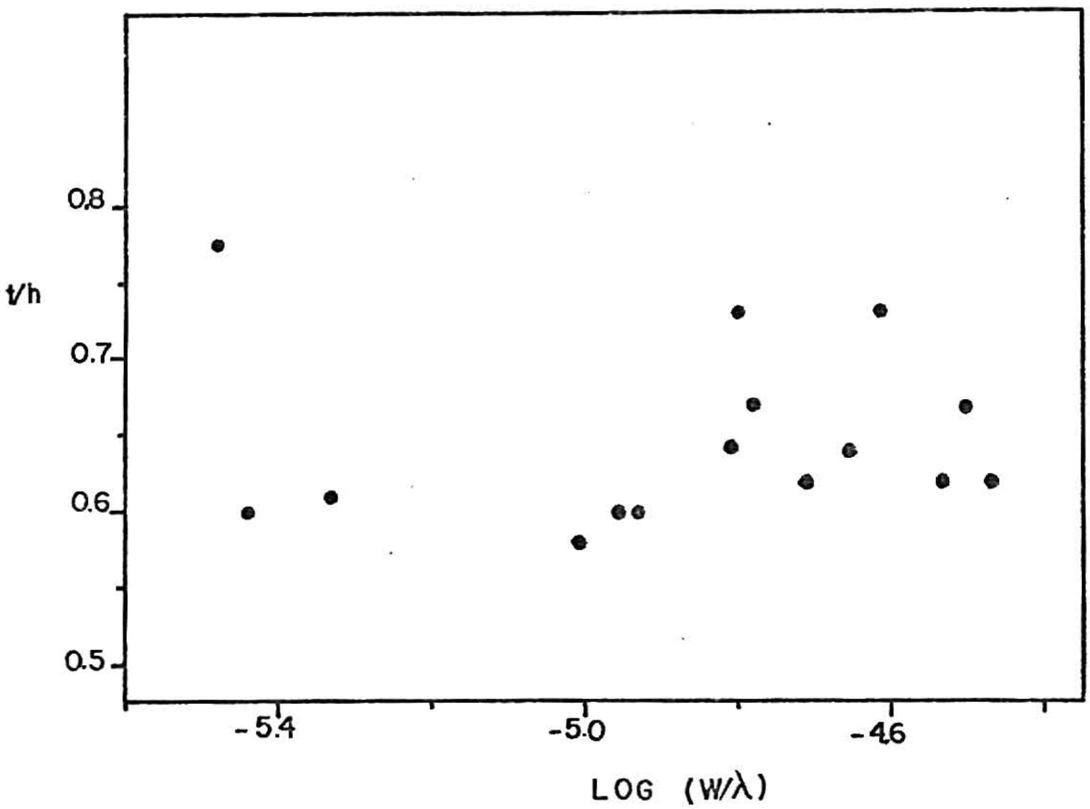

Fig. 20 - Curve of line shape for selected lines in Scorpii, B0V. Data from Hardop and Scholz (1970).

REFERENCES

Abt, H. A. 1958, Ap. J., 127, 658.

Aller, L. H. 1963, "Astrophysics--the Atmospheres of the Sun and the Stars," (2d ed; New York: Ronald Press).

Aller, L. H., Elste, G., and Jugaru, J. 1957, Ap. J. Suppl., 3, 1.

Beckers & Morrison. 1970, BAAS, 2, 182.

Bray, R.J. & Loughhead, R.E. 1967, "The Solar Granulation," (London: Chapman & Hall, Ltd.).

Canfield, R. C. 1971, Solar Physics, 20, 275.

Clauser, F. H. 1961, IAU Symposium #12, Nuovo Chimento Suppl., 22, 129.

Cowley, C. R. 1970, "The Theory of Stellar Spectra, (New York: Gordon & Creach).

deJager, C. and Neven, L. 1967, Solar Physics, 1, 27.

deJager, C. and Neven, L. 1968, Solar Physics, 4, 379.

Elste, G. 1968, The Quiet Photosphere and Ion Chromosphere, ed (deJager), (Dordrecht--Holland, D. Reidel Publishing Co.), p. 106.

Elste, G. 1967, Ap. J., 148, 857.

Elvey, C. T. 1934, Ap. J., 74, 263.

Foy, R. 1972, Astr. Astrophys., 18, 26.

Garz, Holweger, Kock and Richter. 1969, Astr. Astrophys., 2, 446.

Gonczi, G. & Roddier, F. 1971, Astronomy & Astrophysics, 11, 28.

Gonczi, G. & Roddier, F. 1968, Solar Phys., 3, 106.

Gurtovenko, E. A. and Ratnikova, V. A. 1971, Soviet Astronomy AJ., 14, 845.

Greenstein, J. L. 1970, "Spectroscopic Astrophysics," ed. G. Herbig (Berkeley, Univ. of California Press, 1970), p. 61.

Huang, S. S. 1950, Ap.J., 112, 418.

Huang, S. S. and Struve, O. 1952, Ap. J., 116, 410.

Huang, S. S. and Struve, O. 1953, Ap. J., 118, 463.

Huang, S. S. and Struve, O. 1955, Ap. J., 121, 84.

Huang, S. S. and Struve, O. 1960, Stellar Atmospheres, ed. J. L. Greenstein (Chicago: Univ. of Chicago Press), Ch. 8.

Hardar and Schole, M. 1970, Ap. J. Suppl., 19, 193.

Heintz, Hubenet, deJager, C. 1964, BAN, 17.

Lin, C. C. and Reid, W. H. 1963, Handbook der Physik, 12 (Berlin; Springer-Verlag), p. 438.

Milhalas, D. 1970, Stellar Atmospheres (San Francisco: Freeman & Co.), p. 235.

Noyes, R. W. IAU Symposium, 28.

Slettebak, A. 1956, Ap. J., 124, 173.

Scholz, M. 1972, Astrophys. Lett.,10, 137.

Struve, O. 1946, Ap. J., 104, 138.

Struve, O. and Elvey, C. T. 1934, Ap. J., 79, 409.

Struve, O. and Morgan, W. W. 1932, Proc. National Academy of Sciences, 18, 590.

Schmalberger, D.C. 1963, Ap. J., 138, 693.

van den Heuvel, E. P. J. 1963, BAN, 17, 148.

Underhill, A. P. 1961, IAU Symposium #12, Nuovo Chimento, 22, 69.

Unsold, A. and Struve, O. 1949, Ap. J., 110, 455.

Worrall, G. and Wilson, A. M. 1972a, Nature, 236, 15.

Worrall, G. and Wilson, A. M. 1972b, To Appear in Vistas in Astronomy.

APPENDIX A

STELLAR LINE FORMATION THEORY

a) Line Depth Calculation

A stellar absorption line profile, shown in Figure A1 is usually described in terms of the line depth, r, measured as a function of the wavelength difference, $\Delta\lambda$, from the line center. In terms of the monochromatic continuum intensity, I^c, and the monochromatic line intensity, I^ℓ, the line depth can be written as

$$r(\mu) = \frac{I^c - I^\lambda}{I^c} \qquad \text{(A1)}$$

where μ $(= \cos\theta)$ is the limb distance and θ is the heliocentric position of the area of interest on the solar disk. The star from which we receive the radiation is assumed to be spherically symmetric with an atmosphere stratified in homogeneous, plane-parallel, steady-state layers. One also assumes that the atmospheric layers as a whole may be described as being in hydrostatic equilibrium even though mass motions due occur as observed in the sun. The classical problem of stellar line formation also assumes that the atmosphere is in a state of thermal equilibrium.

From the solution of the transfer equation for the semi-infinite atmosphere (see Aller, 1963 or Cowley, 1970), one obtains the following expression for the emergent monochromatic continuum intensity

$$I^c = \int S^c e^{-\tau^c/\mu} \frac{d\tau^c}{\mu} . \tag{A2}$$

The monochromatic continuum source function, S^c, is the ratio of the mass continuum emission coefficient to the mass continuum absorption coefficient and is a function of depth in the atmosphere. The other terms in the equation are the monochromatic optical depth, τ^c, defined by the integral over all layers above the layer of interest of the monochromatic mass absorption coefficient, K, or

$$\tau^c(s) = \int_0^s \kappa \rho \, ds , \tag{A3}$$

where ρ is the mass density and s is the depth in the radial direction. The optical depth scale is such that a change in optical depth of unity will reduce the intensity of the radiation by a factor of 1/e of its original intensity neglecting re-emission.

Similarly one obtains an expression for the monochromatic line intensity as

$$I^l = \int S \, e^{-\tau/\mu} \frac{d\tau}{\mu} , \tag{A4}$$

where S is the source function for the line intensity and τ is the sum of the continuum optical depth, τ^c , and the line optical depth, τ^l . The dependence of the source function S on continuum and selective absorption and emission processes can be expressed as in the following equation

$$S = \frac{S^c + \eta S^l}{1+\eta} , \tag{A5}$$

where S^l is the ratio of the line monochromatic emission to the line monochromatic absorption coefficients and where $\eta = \kappa^l/\kappa^c$ or the ratio of the line absorption coefficient, K^l , to the continuum monochromatic absorption coefficient. The total absorption coefficient in the line is the sum,

$$\kappa = \kappa^l + \kappa^c \tag{A6}$$

Substituting equations A2 and A4 we can write for the line depth, equation (A1),

$$r(\mu) = \frac{\int S^c e^{-\tau^c/\mu} \frac{d\tau^c}{\mu} - \int S\, e^{-\tau/\mu} \frac{d\tau}{\mu}}{\int S^c e^{-\tau^c/\mu} \frac{d\tau^c}{\mu}} . \tag{A7}$$

We assume local thermodynamic equilibrium, LTE, for which the source function is the Planck function, atomic level populations are determined by the Boltzman equation, and the Saha equation describes the ionization equilibrium (Cowley, 1970). As the source functions both become the Planck function,

$$B = \frac{2hc^2}{\lambda^5} \frac{1}{e^{(hc/kT)} - 1} , \tag{A8}$$

where h is Planck's constant, c is the velocity of light, λ is the wavelength, k is Boltzman's constant, and T is the electron kinetic temperature, equation (A7) can be simplified.

A further simplication arises from using a common variable of integration. Let us choose an optical depth scale at some particular continuum wavelength for the independent variable. We shall use the continuum optical depth at 5000A, τ_0 , as our reference. The relation between this scale and any other monochromatic optical depth scale is

$$d\tau^c = \frac{\kappa^c}{\kappa_0} d\tau_0 , \tag{A9}$$

where K_0 is the continuous mass absorption coefficient at 5000A.

Since the logarithm of the optical depth is nearly proportional to geometrical depth, it is somewhat more physical to use a logarithmic scale. Let $x = \log \tau_0$ therefore

$$d\tau_0 = \frac{10^x}{Mod}\, dx \,, \tag{A10}$$

where $Mod = \log_{10} e = 0.43429.$

Hence rewriting equation (A9) we obtain

$$d\tau^c = \left(\frac{K^c}{K_0}\right)\left(\frac{10^x}{Mod}\right) dx \,, \tag{A11}$$

and similarily for equation (A4) $d\tau$ becomes

$$d\tau = d\tau^c + d\tau^l = \left(\frac{K^c + K^l}{K^c}\right) d\tau^c$$

$$= (1+\eta)\left(\frac{K^c}{K_0}\right)\left(\frac{10^x}{Mod}\right) dx \,. \tag{A12}$$

Therefore we can now substitute the above into equation (A7) and write for the line depth,

$$r(\mu) = \int_{-\infty}^{\infty} \frac{B}{I^c} e^{-\tau^c/\mu}\left[1 - e^{-\tau^l/\mu}(1+\eta)\right]$$

$$\times \left(\frac{\kappa^c}{\kappa_0}\right)\left(\frac{10^x}{M\alpha}\right) \frac{dx}{\mu} . \tag{A13}$$

The Planckian gradient form can be obtained by taking the general equations for the emergent intensities, integrate them by parts, and then combine them in the line depth equation. This leads to

$$r(\mu) = \frac{1}{I^c} \int_{-\infty}^{\infty} \frac{dB}{dx} e^{-\tau^c/\mu}\left(1 - e^{-\tau^l/\mu}\right) dx . \tag{A14}$$

b) Curve of Growth Theory

The theory and application of the curve of growth technique is discussed in depth in many places (see Greenstein, 1970; Cowley, 1970). Only a brief description of the formulation used in this study will be given here.

There are several formulations of the curve of growth which most often takes the form of a plot of the equivalent width of the line on the ordinate and some quantity proportional to the number of absorbing atoms on the abscissa. The equivalent width, W , is defined as the integral of the line depth over the entire profile or

$$w = \int_{-\infty}^{\infty} r \, d\lambda \, . \tag{A15}$$

A very useful form, especially for theoretical calculations, is to plot the logrithm of the equivalent width divided by the wavelength, log (w/2), on the ordinate against the logrithm of the unsaturated equivalent width divided by the wavelength, log $(w/\lambda)^*$ (Aller, Elste, and Jugaku, 1957). The division by the wavelength removes any wavelength dependence due to the Doppler effect.

One can show that the unsaturated equivalent width is directly proportional to the number of absorbing atoms (Aller, 1967). The unsaturated equivalent width is given by

$$\log (w/\lambda)^* = \log \epsilon + \log gf\lambda + \log L_\lambda \, , \tag{A16}$$

when ϵ is the ratio of the number of atoms of the element of interest to the number of hydrogen atoms, g is the statistical weight of the level of interest and f and λ are the oscillator strength and wavelength respectively of the transition of interest. The atomic level populations are contained in the L_λ term whose value is dependent on the model atmosphere used. Thus the abundance, log ϵ , term can be easily separated out and we may write

$$\log (W/L)^* = \log \epsilon + \log C , \tag{A17}$$

when the log C contains all the atomic and model dependent quantities. This is the form of the curve of growth utilized in this study.

APPENDIX B

NUMERICAL INTEGRATION OF INTENSITY PROFILES

The monochromatic flux in either the continuum or line is defined as the intensity (see Appendix A) integrated over the visible surface of a star, which can be written as

$$\pi F = 2\pi \int_0^{2\pi} I(\mu) \cos\theta \sin\theta \; d\theta, \tag{B1}$$

or substituting equation (A2) and assuming LTE

$$\pi F = 2\pi \int_0^{2\pi}\int_0^{\infty} B \; e^{-\tau/\mu} \frac{d\tau}{\mu} \cos\theta \sin\theta \; d\theta \; . \tag{B2}$$

Now if we let $\sec\theta = y$, then

$$\frac{dy}{\sec^2\theta} = \sin\theta \; d\theta . \tag{B3}$$

Thus substituting dy/y^2 and changing the limits of integration we obtain the equation

$$\pi F = 2\pi \int_0^\infty B \left[\int_1^\infty \frac{e^{-\tau\gamma}}{\gamma}\, d\gamma \right] d\tau , \tag{B4}$$

where the quantity in brackets is the second exponential integral, $E_2(\tau)$ (see Aller,1963).

Alternately equation (B1) can be written in terms of

as

$$\pi F = 2\pi \int_0^1 I(\mu)\, \mu\, d\mu ,$$

$$F = 2 \int_0^1 I(\mu)\, \mu\, d\mu . \tag{B5}$$

This form of the flux equation is employed as it is more suitable to numerical integration since the quantity I(μ) can be obtained from the expression for the intensity line depth. The flux line depth is defined as

$$R = \frac{F^c - F^\lambda}{F^c} \tag{B6}$$

where F^c is the monochromatic continuum flux and F is the monochromatic line flux. Since the continuum flux does not vary appreciably over the wavelength interval of the line profile

$$R = \frac{\int_0^1 (I^c - I^\ell)\mu\, d\mu}{\int I^c \mu\, d\mu}$$

$$= \frac{2}{F^c} \int_0^1 I^c r \mu\, d\mu , \tag{B7}$$

where r is the intensity line depth (see Appendix A). Let us rewrite equation (B7) as

$$F = 2 \int_0^1 G(\mu)\, d\mu , \tag{B8}$$

where $G(\mu) = I^c r \mu / F^c$. Equation (B8) can be integrated by several simple techniques. By looking at the behavior of $G(\mu)$ for several different $\Delta\lambda$'s from the line center (see Figure B1) one can choose trial techniques to maximize accuracy. The following trials were made.

Explanation of Plate XI

Fig. B1. The integrand, G, is plotted as a function of μ for various values of $\Delta\lambda$ from line center. Note the linear behavior near disk center.

Fig. B2. The percent error, δ, is plotted as a function of line depth, R, for both the 5 and 10 point trapezoidal integration schemes.

PLATE XI

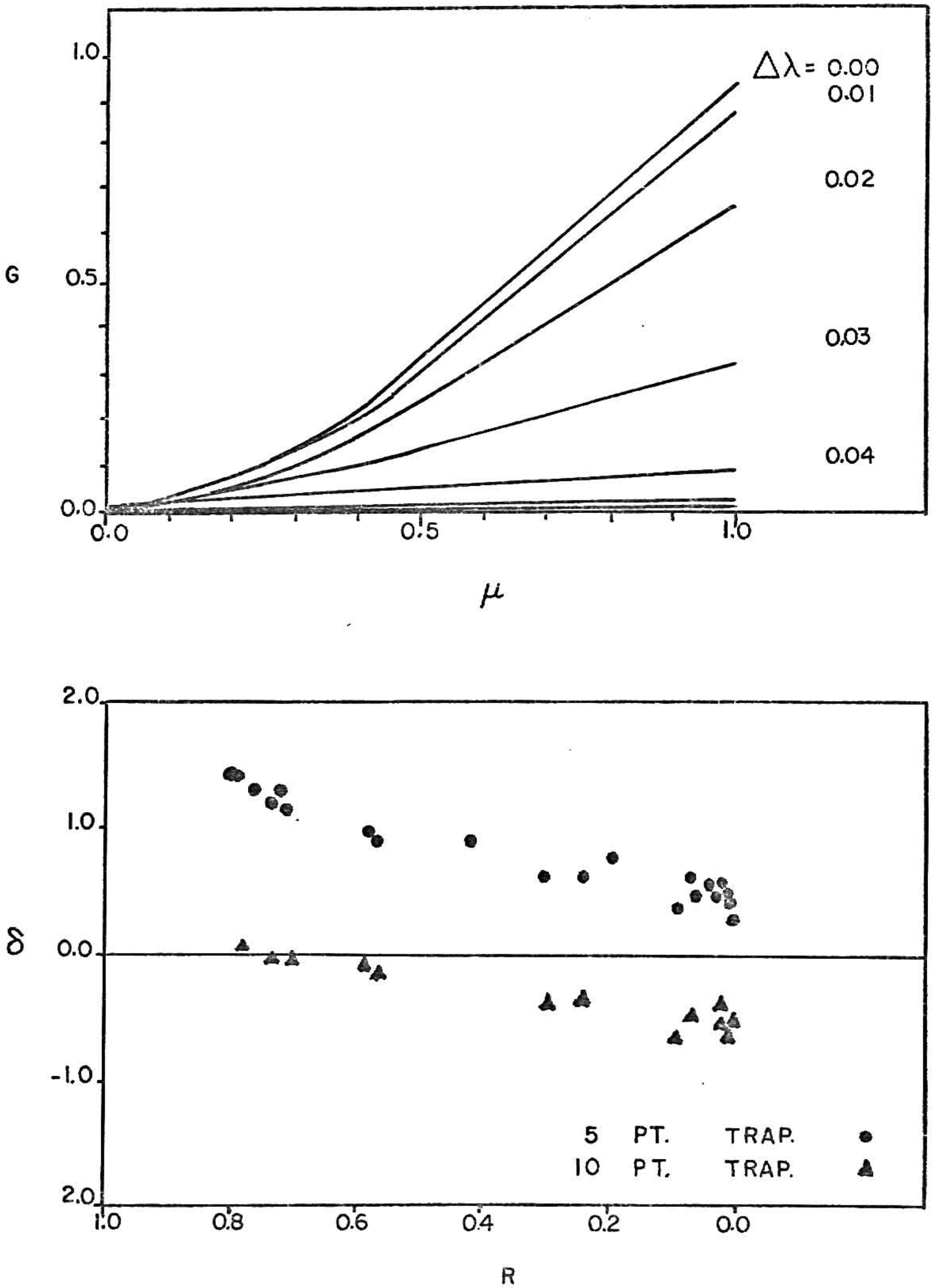

1.0
G
0.5
0.0
0.0
0.5
1.0
μ
$\Delta\lambda$ = 0.00
0.01
0.02
0.03
0.04
2.0
1.0
δ
0.0
-1.0
2.0
1.0
0.8
0.6
0.4
0.2
0.0
R
5 PT. TRAP.
10 PT. TRAP.

1) First a trapezoidal integration was tried. Values at ten limb distances, μ = 1.0, 0.90 ... 0.10, were used to obtain the flux line depth. We have the expression

$$R_{TRAP} = 2\left\{\frac{0.1}{2}\left[G(1.0) + 2\,G(0.9 + \cdots\right.\right.$$

$$\left.\left.+ 2\,G(0.2) + G(0.1)\right]\right\}. \tag{B9}$$

2) In the following three trials profiles were computed using only points at μ = 1.0, 0.7 and 0.4. Also implicitly considered was a point for μ = 0.0 for which G(o) is assumed to be zero.

i) The approximation discussed here uses a separate trapezoidal integration over the intervals μ = 1.0 to μ = 0.4 and μ = 0.4 to μ = 0.0. The line depth for this trial, termed R_{TC}, is given by

$$R_{TC} = 2\left\{\frac{0.3}{2}\left[G(1.0) + 2\,G(0.7) + G(0.4)\right]\right.$$

$$\left.+ \frac{0.4}{2}\left[G(0.4)\right]\right\}. \tag{B10}$$

ii) The same combination as in (i) over the same intervals is used here only with a Simpson's rule integration in the interval $\mu < 0.4$. Thus the line depth here, R_{ST}, is

$$R_{ST} = 2\left\{ \frac{0.3}{2}\left[G(1.0) + 2\,G(0.7) + G(0.4) \right] + \frac{0.4}{3}\left[G(0.4) \right] \right\}. \tag{B11}$$

iii) This trial is similar to the above two with the exception that Simpson's rule is employed for both intervals. Thus

$$R_{SS} = 2\left\{ \frac{0.3}{3}\left[G(1.0) + 4.0\,G(0.7) + G(0.4) \right] + \frac{0.4}{3}\left[G(0.4) \right] \right\}. \tag{B12}$$

3) Next line depths where calculated using four computed points and the implicit point at $\mu = 0.0$. The computed points are at $\mu = 1.0$, 0.7, 0.4, and 0.2. The integrations are again done over two distinct intervals, $1.0 \leq \mu \leq 0.4$ and $0.4 \leq \mu \leq 0.0$.

i) Using Simpson's rule for both intervals we obtain

$$R_{SS} = 2\left\{ \frac{0.3}{2}\left[G(1.0) + 4\,G(0.7 \;+\; G(0.4)\right] \right.$$

$$\left. + \frac{0.2}{3}\left[G(0.4) + 4\,G(0.2)\right] \right\} . \qquad \text{(B13)}$$

ii) Using a combination of a Simpson and trapezoidal integration over the intervals $1.0 \leq \mu \leq 0.4$ and $0.4 \leq \mu \leq 0.0$ respectively we have

$$R_{ST} = 2\left\{ \frac{0.3}{2}\left[G(1.0) + 2\,G(0.7) + G(0.4)\right] \right\}$$

$$+ \frac{0.2}{3}\left[G(0.4) + 4\,G(0.2)\right] \Big\} . \qquad \text{(B14)}$$

4) The final trial uses five computed points at $\mu = 1.0$, 0.8, ... 0.2 and the point at $\mu = 0.0$. For a trapezoidal scheme we have

$$R_{TRAP} = 2\left\{ \frac{0.2}{2}\left[G(1.0) + 2\,G(0.8) + \cdots + 2\,G(0.2)\right] \right\} . \qquad \text{(B15)}$$

The errors in the integrations are a function of the line depth. The errors, ϵ, are the percentage error between the numerical calculation and an identical calculation using the analytical expression for line depth, and are displayed for the schemes tried in Figures B2, B3 and B4.

The somewhat surprising result is that a four point integration scheme, as in paragraph (3i), yields results which are comparable to those obtained with schemes employing more points. Thus one gains very little in computing large numbers of points for a problem where the profile is not expected to change in different directions from the center of the stellar disk.

Explanation of Plate XII

Fig. B3. The same data as in Figure B2 is displayed for the three point integration schemes.

Fig. B4. Error data for the four point schemes are shown.

PLATE XII

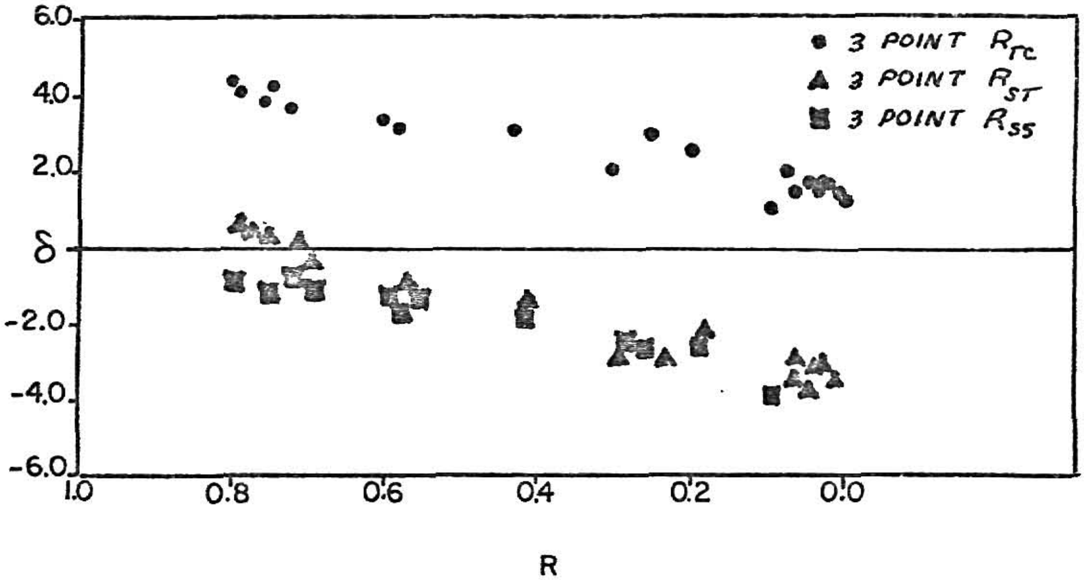

6.0
4.0
2.0
δ
-2.0
-4.0
-6.0
1.0
0.8
0.6
0.4
0.2
0.0
R
3 POINT R_{TC}
3 POINT R_{ST}
3 POINT R_{SS}

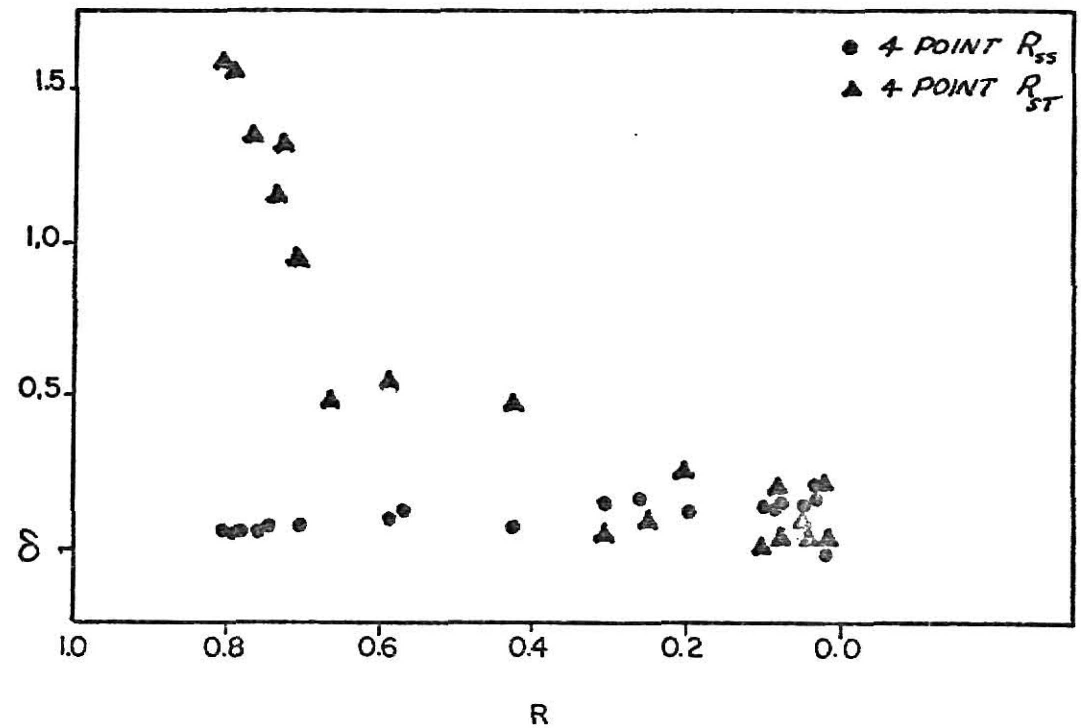

1.5
1.0
0.5
δ
1.0
0.8
0.6
0.4
0.2
0.0
R
4 POINT R_{SS}
4 POINT R_{ST}

THE EFFECTS OF NON-THERMAL VELOCITY FIELDS
ON SOLAR LINE PROFILES

by

LAWRENCE WILLIAM RAMSEY

B.A., University of Missouri, St. Louis, 1968

AN ABSTRACT OF A MASTER'S THESIS

submitted in partial fulfillment of the

requirements for the degree

MASTER OF SCIENCE

Department of Physics

KANSAS STATE UNIVERSITY

Manhattan, Kansas

1972

Velocity fields on a small scale, microtrubulence, and on a large scale, macroturbulence, are often used in both solar and stellar spectrum analysis. There is some question as to the relative importance of these mechanisms in line formation. In order to help resolve this question detailed calculations have been made of solar line profiles for several microturbulence and large scale velocity field models. A new method for calculating profiles broadened by large scale velocity fields is also introduced. The results of the calculations are analyzed using a curve of line shape and it is shown that for a broad range of models the line formed in small scale velocity fields are quantitatively and qualitatively different than those formed in large scale velocity fields.